A THESIS SUBMITTED TO
THE GRADUATE SCHOOL OF NATURAL AND APPLIED SCIENCES
OF ÇANKIRI KARATEKİN UNIVERSITY

A HYBRID OF CNN AND PCA IN SKIN CANCER FOR IMPROVING ACCURACY DETECTION

IN PARTIAL FULFILLMENT OF THE REQUIREMENTS
FOR
THE DEGREE OF MASTER OF SCIENCE
IN
ELECTRICAL AND ELECTRONICS ENGINEERING

BY

MOHAMMED HANI SHAKIR KFASHI

ÇANKIRI

2022

A HYBRID OF CNN AND PCA IN SKIN CANCER FOR IMPROVING ACCURACY DETECTION

By Mohammed Hani Shakir KFASHI

May 2022

We certify that we have read this thesis and that in our opinion it is fully adequate, in scope and in quality, as a thesis for the degree of Master of Science

Advisor **:** Asst. Prof. Dr. Zafer CİVELEK

Examining Committee Members:

Chairman **:** Assoc. Prof. Dr. Murat LÜY
Electrical and Electronics Engineering
Kırıkkale University

Member **:** Asst. Prof. Dr. Fuat TÜRK
Computer Engineering
Çankırı Karatekin University

Member **:** Asst. Prof. Dr. Zafer CİVELEK
Electrical and Electronics Engineering
Çankırı Karatekin University

Approved for the Graduate School of Natural and Applied Sciences

Prof. Dr. İbrahim ÇİFTÇİ
Director of Graduate School

I hereby declare that all information in this document has been obtained and presented in accordance with academic rules and ethical conduct. I also declare that, as required by these rules and conduct, I have fully cited and referenced all material and results that are not original to this work.

Mohammed Hani Shakir KFASHI

ABSTRACT

A HYBRID OF CNN AND PCA IN SKIN CANCER FOR IMPROVING ACCURACY DETECTION

Mohammed Hani Shakir KFASHI
Master of Science in Electrical and Electronics Engineering
Advisor: Asst. Prof. Dr. Zafer CİVELEK

May 2022

Cancer is a generic term for many diseases that can affect any part of the human body. Skin cancer is considered to be the greatest common and dangerous type of cancer. Information technology techniques are required to detect and diagnose skin cancer. Therefore, there is a essential for an early and accurate diagnosis and treatment of skin cancer using effective and deep learning techniques. This research work proposes automatic diagnosis of skin cancer by employing Deep Convolution Neural Network (DCNN). The distinguishing feature of this research is it employs DCNN with 12 nested processing layers increasing the diagnosis and detection of skin cancer accuracy. Moreover, it can detect the cancer if it is malignant or benign in the early stages with high accuracy. Beside neural network, machine learning techniques of Naive Bayes and random forest are also utilized to detect skin cancer. This research work results concluded that the deep learning technique are more effective than machine learning in terms of skin cancer detection. By applying Naive Bayesian on the proposed system accuracy of 96% were achieved, similarly for Random forest method, an accuracy of 97% were achieved. The accuracy of 99.5% were achieved by applying Deep CNN network.

2022, 76 pages

Keywords: Skin cancer, Machine learning, Deep learning and detection, Diagnosis,

ÖZET

DOĞRULUK TESPİTİNİ İYİLEŞTİRMEK İÇİN CİLT KANSERİNDE CNN VE PCA HİBRİTİ

Mohammed Hani Shakir KFASHI
Elektrik ve Elektronik Mühendisliği, Yüksek Lisans
Tez Danışmanı: Dr. Öğr. Üyesi Zafer CİVELEK

Mayıs 2022

Kanser, insan vücudunun herhangi bir bölümünü etkileyebilen birçok hastalığın genel adıdır. Cilt kanseri en yaygın ve tehlikeli kanser türü olarak kabul edilir. Cilt kanserini tespit etmek ve teşhis etmek için bilgi teknolojisi teknikleri gereklidir. Bu nedenle, etkin ve derin öğrenme teknikleri kullanılarak erken ve doğru bir cilt kanseri teşhisi ve tedavisine ihtiyaç vardır. Bu araştırma çalışması, Derin Evrişim Sinir Ağı (DPD-DCNN) kullanarak cilt kanserinin otomatik teşhisini önermektedir. Bu araştırmanın ayırt edici özelliği, cilt kanseri doğruluğunun teşhisini ve tespitini artıran 12 iç içe işleme katmanına sahip DCNN kullanmasıdır. Ayrıca kanserin kötü huylu veya iyi huylu olup olmadığını erken evrelerde yüksek doğrulukla tespit edebilmektedir. Sinir ağının yanı sıra, cilt kanserini tespit etmek için Naive Bayes ve rassal orman makine öğrenme teknikleri de kullanılmaktadır. Bu araştırma çalışması sonuçları, derin öğrenme tekniğinin cilt kanseri tespiti açısından makine öğreniminden daha etkili olduğu sonucuna varmıştır. Önerilen sistem doğruluğuna Naive Bayes uygulanarak %96'lık bir doğruluk elde edildi, benzer şekilde rassal orman yöntemi için de %97'lik bir doğruluk elde edildi. Deep CNN ağı uygulanarak %99,5 doğruluk elde edildi.

2022, 76 sayfa

Anahtar Kelimeler: Cilt kanseri, Makine öğrenimi, Derin öğrenme ve algılama, Teşhis

PREFACE AND ACKNOWLEDGEMENTS

Upon closer inspection of this significant work, we can discover that it comprises the efforts of a number of people. I want to express my gratitude to everybody from the depth of my soul, and to express that however much I cherish and respect their decision. A special thanks goes out to Asst. Prof. Dr. Zafer CİVELEK for his assistance in the supervision of my thesis. I owe him a sense of gratitude for granting time and resources required to pursue a master's degree. I learned a great lot from him both intellectually and professionally, and I am grateful to him for his guidance.

I give a debt of gratitude to all those who have assisted me to get to where I am presently. It is impossible to express my appreciation enough to my wonderful parents, and grandparents for all efforts and unquestioning support throughout my life.

I am thankful for the support and motivation I received from Mr. Bashar A. Al-KHAYAT.

I would like to express my gratefulness and my full-hearted thank for my family for all of their sacrifices that have made on my behalf.

Mohammed Hani Shakir KFASHI

Çankırı-2022

CONTENTS

LIST OF SYMBOLS

$\cap$	Intersection symbol
$\cup$	Union symbol
$\vert$	Such that
π	Pi value
Σ	Sigma
σ	Sigma
ω	Omega

LIST OF ABBREVIATIONS

ANN	Artificial neural network
CNN	Convolution neural network
DCNN	Deep convolution neural network
HIS	Hue-saturation-intensity
HSL	Hue-saturation-lightness
HSV	Hue-saturation-value
KNN	K-nearest neighbors
PCA	Principal component analysis
PNN	Probabilistic neural network
RGB	Red green blue
SVM	Support vector machine

LIST OF FIGURES

LIST OF TABLES

1 INTRODUCTION

1.1 General Overview

Cancer is a general term representing variety of diseases effecting any part of human body. Other terms are also used for cancer such as neoplasms and malignant tumor. The cancer most distinguishing characteristics is the aberrant cells prompt formation that expand past their normal borders and can later infiltrate adjacent shares of the body and migrate to other organs, a process known as metastasizing. Metases is the main cause of death in cancer disease. In the year 2018, approximately 9.6 million people died of cancer which is one in every six death ratio (Daghrir *et al.* 2020).

Skin cancer has recently been identified as the most dangerous kind of cancer seen in humans. Melanoma, Basal and Squamous cell Carcinoma are three kinds of skin cancer, with Melanoma being the greatest unforeseen. In general skin cancer cases is increasing in recent years for both cases of non melanoma and melanoma. According to the reports non melanoma cancer cases are around 3 million occure in a single year, while melanoma cancer cases are 132.000 per year globally. Skin cancer is identified in one out of every three cancers, and one out of every five Americans will acquire skin cancer throughout their lifetime, according to Skin Cancer Foundation statistics. Skin cancer, often known as melanoma, is the 19th greatest prevalent malignant cancer in both men and women. Almost 300.000 new cases were stated in 2018. Non-melanoma skin cancer is the fifth greatest recurrent distortion in men and women, with more than 1 million cases in 2018 (Rock *et al.* 2020). Furthermore, due of its likeness, clinicians face the greatest difficulty in detecting and diagnosing cancer sickness. At its first stages, skin cancer is as little as a mole, making it impossible to detect with the naked eye (Younis *et al.* 2019)

In disease diagnostics, information technology plays a major role. Advancements in information technology open up a plethora of possibilities for bettering healthcare delivery in the areas of diseases diagnosis, management, and support. Enhanced automatic decision support systems, in combination with evidence-based medicine, are the foundation for crucial diagnostic aids (Hudson and Cohen 2003).

Using information technology, several well-established research in skin cancer detection and diagnosis have been established. Machine knowledge procedure e.g. SVM, Naive Bayes, Agent technology, and Neural Network were utilized by some of them (Monika *et al.* 2020). Whereas, Deep learning approaches such as PNN, ANN, and CNN have shown the greatest results in skin cancer discovery and analysis (Hu *et al.* 2018)

The classic image classification approach necessitates the depiction of salient characteristics for training the classifier. These properties can be texture, colour, or form of colour pictures, however extracting the elements and classifying an image based on them is difficult in the case of skin cancer. Researchers are encouraged to employ deep convolution neural networks (CNNs) to extract topographies. New research has demonstrated that CNNs can reliably extract high-level (semantics and texture) and low-level (edges and forms) information owing to the abstraction capability of its layers (Younis *et al.* 2019). However, according to the research, using CNN to identify and diagnose skin cancer produces the greatest outcomes. Therefore, in this work, Deep CNN will be employed for skin cancer diagnosis and detection.

1.2 Problem Statement

Skin cancer is described as the irregular cells uncontrolled development in the epidermis, the furthest layer of skin, caused by uncorrected DNA damage that results in mutations. Skin cancer is a dangerous and widespread disease. A conventional way for identifying skin cancer is a biopsy. This procedure is both uncomfortable and intrusive. This procedure necessitates laboratory testing, which takes time. As a result, computer-assisted skin cancer diagnosis is required to address the aforementioned difficulties. The suggested technique allows clinicians to obtain precise and speedy results at an initial phase, which boosts the survival rate.

1.3 Thesis Objectives

The aim of this work is to design an accurate system for skin cancer diagnosis and detection, and it is summarized as follows:

(i) To design and implement an early and accurate skin cancer discovery system by usage a deep Convolution Neural Network algorithm.

(ii) To design and implement an accurate and early system for sckin cancer detection based on the most effective machine learning algorithms which are Random Forest, and Naive Bayes.

(iii) Test the proposed model performance then evaluation on the basis of accuracy, then compare the obtained results with each other and with the related work.

1.4 Research Scope

The module is usage to notice and diagonsis skin cancer based on deep neural network using DCNN. The scope of this work is as follows.

(i) This study focused on skin cancer detection and diagnosis accurately at early stage.

(ii) With regards to skin cancer, this work focuses on detection and diagnosis melanoma that is the greatest common and unsafe kind of skin cancer. Since it can effortlessly affect the other parts of the body.

(iii) This work is designed based on the deep learning using the well known DCNN algorithm. Deep knowledge is a division of mechanism knowledge in which false neural networks, or techniques human brain inspired, enable machines to solve complicated issues even when working with large, interconnected, and unstructured data sets. Skin cancer diagnosis might be aided by deep learning classifiers.

(iv) The most effictave mechanism knowledge methods which are Random Forest, and Naive Bayes are selected to design, implement, test and evaluate.

(v) In this work, Python has been used to simulate the proposed system. Furthermore, the data utilised in this study comes from the ISIS dataset, which was obtained at the Hospital Pedro Hispano's Dermatology Service under comparable conditions utilising a Tuebinger Mole Analyzer system with a magnification. The dataset covers 200 photos, with 80 images belonging to a kind tumor, other suspicious lesion are 80 images and the remaining malignant lesion are 40 images. The dataset comprises 200 photos, 40 of which are of a malignant lesion and 80 of which are of a benign lesion.

1.5 Thesis Contribution

In this work, an precise system for skin cancer diagnosis and discovery is proposed. The proposed system is founded on the effective deep learning techniqus which is Deep Convlutioanl Neural Network. Our work distungush it self from the priviouse work by increasing the CNN layers which will increase the detection and diagnosis accuracy. Also, two finest machine learning algorithms in this sector, Random Forest, Naive Bayes are created for detecting cancer disorders. The PCA algorithm was used for eye removal. The results for all of Deep and Machine learning was compared with each other, then compired with the related work.

1.6 Thesis Organization

The other chapters in this thesis are: Chapter Two presents the theoretical and mathmatical background of the work.

In this chapter the review and background of pattern detection system, data mining techniques, deep learning, the concept of Skin cancer are discussed in detail.

Chapter Three: The proposed system methodology and architecture.

The suggested system for skin cancer diagnosis, as well as its design and execution, are described in this chapter.

Chapter Four: the results of the proposed syetm and discussion

This chapter discusses the outcomes and evaluations that the suggested system has yielded.

Chapter Five: In this chapter Conclusions and Recommendations for Future Research are presented

This chapter presents the conclusions of this work. Furthermore, future work recommendation are also provided

2 THEORETICAL BACKGROUND

2.1 Introduction

On a daily basis, the number of reported cancer cases has been steadily increasing Early-stage skin cancer can be readily cured with simple procedures or methods, while advanced skin cancer cannot be efficiently treated with medicines As a result, it is critical to diagnose and treat illness at an early stage. (Younis *et al.* 2019) Treatment of BCC involving the nose, lower eyelids, or ears is called primary radiotherapy. The absence of histological control of margins and faults in radiotherapy is a shortcoming that frequently leads to insufficient or excessive treatment. The morpheaform of BCC has been discovered to be resistant to radiation. Early identification of skin cancer is therefore critical for cure, particularly in malignant melanoma (Monika *et al.* 2020). Furthermore, recent technological advancements and huge cost reductions in the field of digital image collection have enabled the practical implementation of a variety of image based diagnostic procedures.

This chapter explains the theoretical foundations of this project. Subsection 2.2 discusses skin cancer, whereas subsection 2.3 discusses data mining. The part on image preparation, on the other hand, has been illustrated section 2.4. In addition, under subsection, the definition of artificial intelligence and its function in image processing has been described in section 2.5. Lastly, the assessment techniques were explained and shown in section 2.6.

2.2 Skin Cancer

Now a days in the world the skin cancer is careful to be the sixth greatest common kind of cancer. Skin is made up of cells, and these cells brand up tissues. As a result, cancer is shaped by abnormal or uncontrolled cell proliferation in the connected tissues or other neighbouring tissues. UV light exposure, a weakened immune system, a family history of cancer, and other issues might all have a role in the development of cancer. These are the ones who make the tissues cancerous (Hu *et al.* 2018). According to the Cancer Council, about two out of every three persons in Australia will be diagnosed with skin cancer. The most prominent skin cancer kinds are Squamous cell carcinoma, melanoma, and basal cell carcinoma. Melanoma, which may spread and infect other organs, is the worst of them all (Jain and Pise 2015)

The survival rate of patients is significantly higher if it is diagnosed in its early stages of development. Visual examination is now the most often used method of screening. However, this necessitates extensive physician training, and the percentage of proper detection remains low (Mansutti *et al.* 2018). As a result, a accurate and reliable method capable of identifying skin cancer early in its growth is required.

2.3 Data Mining

“An iterative method of retrieving data concealed from enormous volumes of raw data,” is known as data mining. It's a tool for predicting future outcomes by extracting knowledge from previous data (Bayati and Jabbar 2015). It is a tool that extracts information from previous data to forecast the outcomes of future occurrences (Bayati and Jabbar 2015). Data removal is the procedure of classifying valid relations and patterns in large data sets using complex data analytic techniques. As a result, data mining entails not only data collection and maintenance, but also analysis and forecasting (Kaur and Jindal 2016).

The requirement for extracting and analysing relevant information from data. With data represented, textual, multimedia, and quantitative, formats can all be used for data mining. To test the data, variety of parameters are employed by numerous applications. Track analysis (design in which one event leads to another), categorization, grouping, and forecasting (finding patterns from which credible predictions about future actions may be made) are among them (Kumar *et al.* 2018). Generally data mining algorithm is made up of three elements listed below (Dunham 2003)

2.3.1 The model

The template includes parameters that must be determined by means of the special representational type or method from data for a function selected. The function of the model (clustering, classification) and its representational form (decision trees, linear discriminants).

2.3.2 Criterion of preference

Based on the facts provided, a preference-based criterion for one model or set of parameters. The criteria is usually some kind of model's fitness function for the information, which is balanced by a smoothing component to avoid overfitness or to avoid building a model with too many degrees of freedom for the provided data (Kaur and Jindal 2016)

2.3.3 Search algorithm

Given the data, models, and preference criterion, an algorithm is created to locate certain patterns or designs and parameters (Zahradnikova *et al*. 2015)

2.3.4 Data mining types

Data mining can have divided into two categories (Kaur and Jindal 2016, Dunham 2003)

- **Predictive data mining:** it generates the system model defined by the data given. Within the data set it uses certain variables or fields to forecast uncertain or potential values of other variables of attention.

- **Descriptive data mining:** generates new non-trivial information based on the data set available. This concentrates on the discovery of patterns which will explain the data that people can understand.

2.4 Images Preprocessing

The crucial stage in any machine learning or deep learning system is preprocessing. For data preparation, many strategies have been used. The most popular and effective were employed in this work, and the following is a summary

2.4.1 Gaussian blur

The outcome of image bluring with a Gaussian function in image processing is a Gaussian blur. In literature it is also defined as Gaussian smoothing (Naji and Al-Tuwaijari 2018). It's a common effect in graphics software for visual noise minimizing and reducing details. On the other hand bokeh effect produced by an out-of-focus lens or the shadow cast by an object in normal illumination, so the blurring approach give a smooth blur as transparent screen (Tiwari *et al.* 2013).

In computer vision methods, Gaussian smoothing is also employed as a pre-processing stage to improve visual structures at various scales. See also (Chandel and Gupta 2013) for scale space representation and implementation. The "Gaussian Blur" is achieved by convolutioning a kernel represented by a Gaussian function with the picture pixels (Chow and Paramesran 2016). In the discrete case, the convolution is given by (Tiwari *et al.* 2013), as seen in the Equation (2.1), Equation (2.2) below;

$$f * g[n] = \sum_{m=-\infty}^{\infty} f[m].g[n-m] \tag{2.1}$$

The two-dimensional Gaussian function was utilised to produce the kernel. A is the amplitude,($(x_\sigma.y_\sigma)$ the center, $\sigma x, \sigma y$ the standard deviations in the x and y directions in following function (Yin and Chaoyang 2011)

$$f(x.y) = A.e^{1\left(\frac{(x-x_0)^2}{2\sigma x^2}+\frac{(y-y_0)^2}{2\sigma y^2}\right)} \tag{2.2}$$

The kernel size will now be discussed in more depth in a later section. Figure 2.1 (Mitra and Acharya 2005)shows an example of a Gaussian distribution.

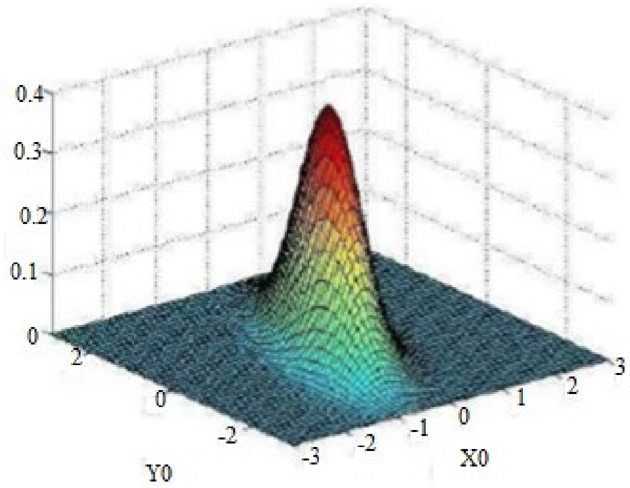

Figure 2.1 Gaussian distribution (Chandel and Gupta 2013, Tiwari *et al.* 2013)

The convolution kernel is used to acquire Gaussian funding in image processing. In the period utilised in the first figure, the distribution values alongside lines are employed to generate a convolution matrix (Kim *et al.* 2006). The weighted normal area of the region is the updated value for each pixel. The initial pixel's value is then set to the highest (the highest Gaussian value), and softer load are assigned to the surrounding pixels as their fields separate from the first (Chandel and Gupta 2013, Kulkarni *et al*. 2014).

2.4.2 Color space

A colour space divides colour data into components on the basis of colour shade. Computer projects, television broadcasts, image processing, and computer vision all employ standard colour spaces (models). To identify the skin, a distinctive colour space is offered (Belgiu and Drăguţ 2016).

RGB based colour space, light based colour space (HSL, HSV, and HSI), and hue based colour space (HSI, HSV, and HSL), are three types (YCBCr, YIQ, and YUV). The next sections go through each of these sorts. The essential skin shading cycle that arises and switches on for characterisation is called defining the shading space. In a given picture, at least one shaded region can offer ideal motion for identifying skin pixels. The positioning system and application of the skin are frequently used to determine the suitable shadow space (Nahata and Singh 2020). To identify skin pixels, the included shadow space is employed.

2.4.2.1 Red, green, and blue (RGB) color model

RGB colour space is extensively utilised and frequently used as evasion colour interplanetary for generating and discussing unique graphics. Some other shadow regions that shift to RGB anyway (Munir *et al.* 2019) Computers, graphics cards, and LCD displays all employ the RGB colour space (Figure 2.2).

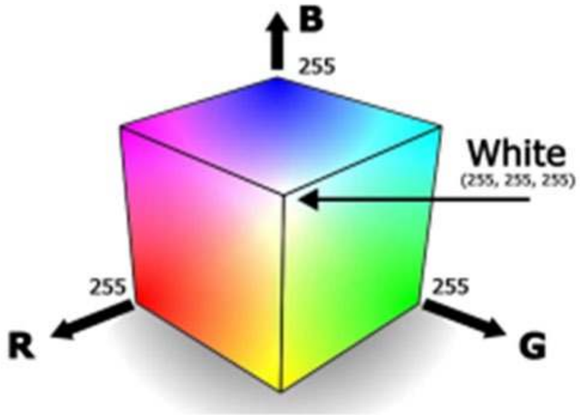

Figure 2.2 Color model RGB (Han *et al.* 2011)

As can be seen in Figure 2.2, it contains of primary Red, Green and blue clolor mechanisms. These three base colours can be utilized to obtain any colour in nature. The newly created colours depends on the mixing ratio of these base colours. Reversing this technique, one can also achieve a specific color by decomposing theses base components as shown in Equation (2.3), Equation (2.4) and Equation (2.5) (Han *et al.* 2011).

$$r = \frac{r}{R+G+B} \tag{2.3}$$

$$g = \frac{g}{R+G+B} \quad (2.4)$$

$$b = \frac{b}{R+G+B} \quad (2.5)$$

2.4.2.2 Luminance, chrominance (YCbCr) color model

YCbCr is a non-linear RGB signal that is widely used in European television studios and for copy reduction. Color is signified by luma (which is brightness determined from nonlinear RGB) formed as a weighted sum of RGB values, as illustrated in Figure 2.3 (Munir *et al.* 2019, Lee *et al.* 2016). In the digital video arena, YCbCr is a widely used colour space. It's utilised in image and video compression formats including JPEG, MPEG1, MPEG2, and MPEG4 since the picture brands it simple to get rid of certain unnecessary colour information (Kingma and Ba 2014). The YCbCr colour space is distinguished by its ease of modification and unambiguous separation of luminance and chrominance components (Santra and Christy 2012, Ibrahim *et al.* 2015)

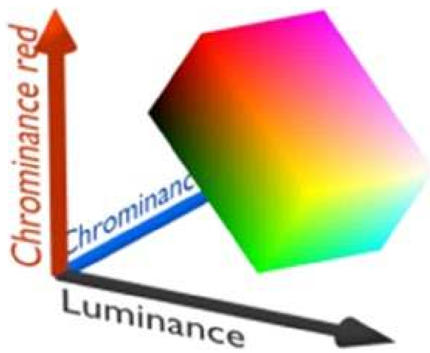

Figure 2.3 YCbCr color model (Kingma and Ba 2014)

The illumination data is divided into one component (Y) and the colour value data into two differentiation sections in this mode (Cb and Cr). Cb discusses the distinction amid the blue section and orientation value. Cr, on the other hand, refers to the polar opposed to red component and reference value. Under conditions Equation (2.6), Equation (2.7), and Equation (2.8), the YCbCr technique may be retrieved from the RGB shading location Equation (2.8).

$$Y=0.299R+0.287G+0.11B \tag{2.6}$$

$$Cr=R-Y \tag{2.7}$$

$$Cb=B-Y \tag{2.8}$$

2.4.3 Fast fourier transform (FFT)

DTFT response is continuous so some mathematical process like multiplication cannot be performend on digital computers. This is extreamly challenging in FFT during multiplication because of the infinite spectrum. With the aid of a digital computer, the samples from the FFT would become simple to multiply. The Discrete Fourier Transform (DFT) is the result (Rasheed *et al.* 2020)

Even though sampling takes place in a discrete frequency domain, while periodic results are obtained in time domain in data sequence (Rasheed *et al.* 2020). Hence, the DFT may be generated by sampling the continuous'ω' at (2π/N)k times, as shown in Equation (2.9) (Gedraite and Hadad 2011)

$$\boldsymbol{x}(\mathrm{k}) = \sum_{\mathrm{n}=0}^{\mathrm{N}-\mathrm{i}} \mathrm{x}[\mathrm{n}]\mathrm{w}_{\mathrm{n}}^{\mathrm{nk}}\ \mathrm{k} = 0.1.2.3.\ldots.\mathrm{N}-1 \tag{2.9}$$

2.4.4 Morphology operations

Mathematical Morphology (MM) is a valuable technique for describing and revealing local forms including edges, shapes, and arching structures. Morphologies also deal with preparation or post-processing, such as morphologies for separating, decreasing, and cutting (Kolkur *et al.* 2017).

Structure projects are deliberate adjustments of pixel quarters and skewed samples basis. Two-dimensional representations surround the majority of the morphology. Morphology projects are a fantastic method to address a variety of imaging demands (Patil and Patil 2012)

The structure elements (SE) decision based digital tasks are known as mathematical morphology (MM). For assembly or drawing files, there is a little layout that is used to display a picture for interesting functions. Because the element in Figure 2.4 exhibits several instances of components, some structural elements (SE) examples are briefly discussed in other ways as well in literature (Kolkur *et al.* 2017).

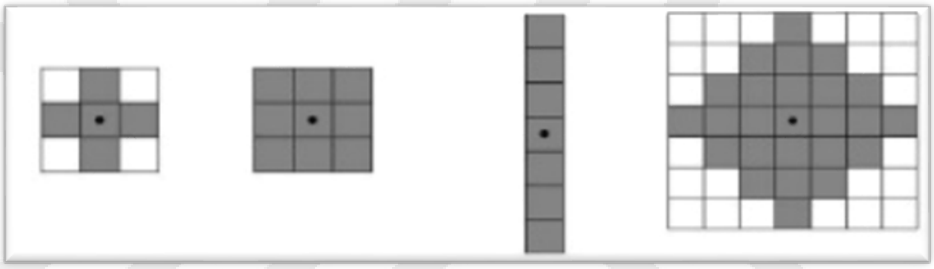

Figure 2.4 Structure elements examples (Rasheed *et al.* 2020, Kolkur *et al.* 2017)

In Figure 2.4 each concealed square represents a component of the (SE). The organisational object origin must be discovered to identify objects which are members of the SE (Patil and Patil 2012). In the figure above, the dark shade of distinct SE classes are likewise shown. The SEs is rectangular arrays, which may be achieved by adding the fewest amount of backdrop elements feasible (Poorani *et al.* 2013)

2.4.4.1 Morphological dilation

In mathematical morphology, there exists two operators one is dilation and other is erosion. The mathematicl morphology is generally used to binary images however it can cover grayscale events are covered as well (Xia *et al.* 2019). The principal effect of the operator on a binary image is to progressively increase the boundaries of foreground pixel regions. As a consequence, foreground pixel areas grow in size, while spaces between them diminish. When we dilate a picture, we increase the white pixel in the image, making it appear larger. Every background pixel that comes into contact with an object pixel becomes an object pixel (Patil and Patil 2012).

The region in the input image is enlarged using dilation. The dilation procedure use SE to probe and extend shapes. The dimension of the matrix is determined by the size of SE, and the form defines a pattern of 1s and 0s (Mecheter *et al*. 2020). The new image I is obtained by employing FE to image A shown in Equation (2.10)

$$I = A \oplus S = \cup_{s \in S} A_s \tag{2.10}$$

2.4.4.2 Opining operation

Using intersection and complementation, the picture opening procedure is a mix of erosion and dilation (Patil and Patil 2012). Assume A is made up of a collection of 8-connected border elements, each of which encloses a backdrop. The process of conditioned dilation startw with matrix X0 of 0 with the same size as A shown below in Equation (2.11)

$$x_{i=}(X_{i-1} \oplus S) \cap A^C \tag{2.11}$$

Where X_i contains total quantity of filled holes

2.4.4.3 Morphological closing

By utilizing the same structuring element the morphological erosion is done (Patil and Patil 2012). Closing operationis defined as shown in below Equation (2.12)

$$A.S = (A \oplus S) \ominus \boldsymbol{S} \tag{2.12}$$

2.4.4.4 Morphological erosion

The images is shrinked by using the morphological erosion operation (Kolkur *et al.* 2017). The image I erosion operation output is shown as Equation (2.13)

$$I = A \ominus S = \bigcap_{s \in S} A_{-s} \tag{2.13}$$

2.5 Artificial Intelligence (AI)

Artificial intelligence (AI) is the the intelligence of machines rather than animals or humans it is also known and machine intelligence. Many AI books describe it as "intelligent agents," study, which are devices that understand their surroundings and perform actions to obtain their objectives simulatinously (Kolkur *et al.* 2017). Machines such as computer simulate "cognitive" activities that people connect with the human mind, like “problem solving” and “learning” are reffered as "artificial intelligence" (Poorani *et al.* 2013).https://en.wikipedia.org/wiki/Artificial_intelligence - cite_note-FOOTNOTERussellNorvig20092-4 In this section, the AI definition has been given with emphasis on machine learning and deep learning as shown in Figure 2.5.

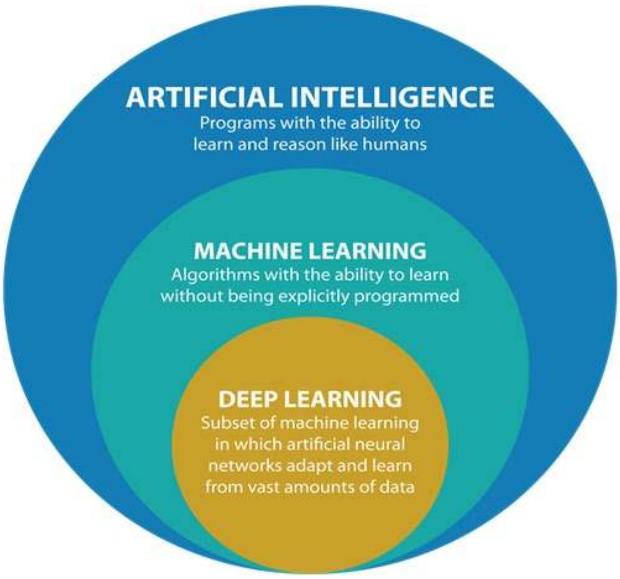

Figure 2.5 The difference between AI, deep learning, and machine learning

Furthermore, while the terms deep learning, machine learning, and artificial intelligence (AI) may appear to be interchangeable, there are significant distinctions between them. One school of thinking holds that artificial intelligence is a broader umbrella term that encompasses both deep learning and machine learning (Kolkur *et al.* 2017). As a result, while everything classified as deep learning or machine learning falls under the artificial intelligence umbrella, not all deep learning and machine learning (Reddy *et al.* 2019). However, this work attempt to employ machine knowledge and deep learning in Skin cancer disease discovery and analysis which shows the power of deep learning in Skin cancer diagnosis and detection.

2.6 Machine Learning

For knowledge discovery (KDD), data mining is the most widely used tecnique of knowledge extraction. Machine learning is a technique that lets a computer to study data, recognise relationships, and apply visions to solve glitches, enhance data, and anticipate consequences (Kaushik *et al.* 2014). Machine learning is a branch of science that studies performance, the theory, and properties of knowledge algorithms and systems (Wang *et al.* 2019).

The research conducted is very interdisciplinary, incorporating topics from AI, optimization theory, statistics, information philosophy, mathematics, and science. Machine learning has impacted practically every scientific field through its use in a wide range of applications (Gobalakrishnan *et al.* 2020). It has had a significant impact on science and society. All of these fields have benefitted, including data removal and informatics, system recognition, autonomous switch engines, recommendation systems. Unsupervised knowledge and supervised learning are the two primary subdomains of machine learning (Wang *et al.* 2019).

- **Supervised learning:**

An objective ability to predict discrete quality values as claimed or not approved. AI computing predicts a specific set of examples when managed to learn computing looks for design in name-oriented information. This algorithm consists of an expected result variable based on a specific set of indicators, e.g. independent variables (Gobalakrishnan *et al.* 2020).

Use this factor scheme to create an equity that manages the contribution to the desired return. The construction process continues pending the model reaches a level of precision in the exercise data. This entire cycle reduces consumption in manual revision of interest and coding. Instances of guided learning: neural networks, decision tree, regression, KNN, logistic regression, SVM, Naive Bayes, etc. (Gobalakrishnan *et al.* 2020).

- **Unsupervised learning:**

Learning a valuable structure without marked classes, improvement rules, feedback signals, or some other info that goes beyond raw data is called unsupervised learning. In this procedure, the absence of an objective variable to evaluate means that there is no selection here related to the information methods, or we can say that the names of the information preparation training data are not clear (Mecheter *et al*. 2020).

This algorithm is used to classify the information in the group collection to represent their structure, for example, to group the information to find important packages and progressive systems. This makes the information fundamental and coordinated for research. Models: K-implies, vague grouping, hierarchical grouping. The information has no name and no known results (Wang *et al.* 2019).

- **Reinforcement learning:**

This is in the middle of the oversaw and unverified knowledge spectrum. The procedure is knowledgeable when the answer is improper, nonetheless not how to precise it. It necessity examine and test numerous options pending it learns how to properly answer the query. Because of the monitor that rates the response but does not proposal changes, strengthening learning is occasionally mentioned to as learning by a detractor (Kaushik *et al.* 2014).

The Classification technique is supervised learning, which predicts each sample's target class in data where the classes are predefined. Organization algorithms need that lessons clear are based on data quality values (Lee *et al.* 2016). The classification process is summarized in two-phase: the first phase represents the training phase while the second phase represents the classification in which the prediction of the data class label by using the model.

The training phase involves building a classifier that describes a previous defined set of data classes, where the organization procedure forms the classifier by knowledge from exercise data and related class labels, this phase can be described as a learning phase where the y = f (x) function will predict the relevant class label for the particular data. Where the accuracy of the prediction is first computed (Mecheter *et al.* 2020). If using the training data for the calculation of accuracy, it will be optimistic (classifier leads to overfitting the data), so in this state, a test set is used where this data is independent of the training set (Olbrys and Mursztyn 2019). If the correctness of the classifier is satisfactory when use the testing set, it can be usage in the upcoming for the data whose class label is unknown (Shrestha and Mahmood 2019). Figure 2.6 give an example of skin cancer classification.

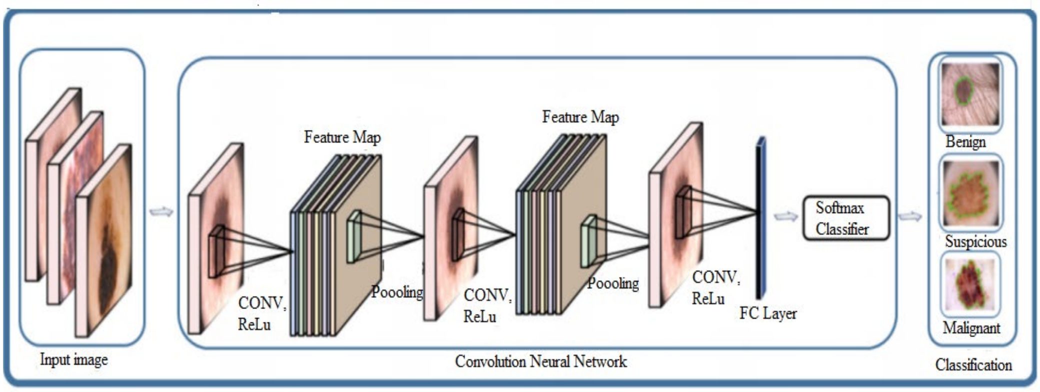

Figure 2.6 Example of skin cancer classification (Saba 2020)

The largest amount of effort in the supervised classification is made before the actual classification. Classification supervised may be much more reliable than classification without supervision, but relies heavily on training, misclassifications will be found (Al-Azawee *et al.* 2015). Supervised categorization necessitates paying particular attention to the generation of training data. The organization consequences would be poor if the exercise data were poor or non-representative. As a result, oversaw organization often involves more money and effort than uncontrolled organization (Olbrys and Mursztyn 2019). However, the current research work employed two operational machine learning algorithms for Skin illnesses diagnosis and detection and which are Random Forest and Naive Bayes.

2.6.1 Naive bayes

The most frequent classification algorithms are naive Bayese approaches, which are based on Bayesian probability theory (Kumar *et al.* 2020). The number obtained by instances A number by total number of events is the probability of an event A. The value of likelihood always lies in between 0 and 1 and are represented as percentage values (Boman and Volminger 2018).

For instance, the likelihood of picking a letter C, D, E, F, G, or H at random is p (sound) = 1/6, or roughly 16.67 percent. Because they have no influence on one other, the probability principle has two independent events. the probability of P(A) and P(B) specified events A and B, explanation of independent events, with conditional likelihood of B resulting in A equaling likelihood of B as shown in Equation (2.14) (Zhang *et al.* 2019).

$$P\,(B \mid A) = p\,(A).\,(B)/\,P\,(A) \qquad (2.14)$$

Thomas Bayes' (1702-1761) understanding of the Bayesian technique had a major influence on the Bayesian notion. The author theory of Bayesian technique were published in the Philosophical Transactions of the Royal Society of London after his demise in 1763 in a paper titled "On the Problem of Opportunity" (Gikunda and Jouandeau 2019). Bayesian statistics is related with calculating the liklihood of a specific pattern (sample) X state that a large number of observations.

The propability posterior (the liklihood of specific class I) or hypothesis is determined in the following Equation (2.15) for pattern X (Gikunda and Jouandeau 2019).

h, P (h|X), is as directed P (h|X) $=\frac{P(X|h)P(h)}{P(X)}$ (2.15)

P (h) $=\frac{|h|}{N}$ are those assessed from the prior probability of h (provided that |h| are patterns in class h and N is total patterns, and all theories have equal chances), P (X|h) is probability of X which is conditional and is dependent over h, and previous probability of X is constant and denoted by P(X). The maximum posterior hypothesis is referred to as the posterior maximum hypothesis (MAP),where assumptions set are represented by H as shown in Equation (2.16) and Equation (2.17)

$P\frac{h}{X}$ h. Class (2.16)

$$h_{MAP} \equiv \arg\max_{h \in H} = \arg\max_{h \in H} P(X|h)P(h) \quad (2.17)$$

The Bayesian classifier can effectively accomplish the least error rate due to the delivery of data probability. The conditional risk (i.e. the predicted loss of a choice) is the lowest here. The optimal classification rule statistically is a standard by which different rating algorithms' output may be compared (Singh *et al.* 2016)

This is a well-known probabilistic classifier that is utilised in a variety of requests. The Bayes classifier is dependent on Bayes theorem, and taking data set characteristic independent naive adjective is generated. In light of the class context, all aspects of the training samples are presumed to be independent of each other (Arora and Agrawal 2020). The NB classifier shows every patterns of n-dimensional X vector for attributes value of [a1, a2... and], assuming that c1, c2... cn. When and only when class C I is allocated to an unknown pattern X, the classificator expects it to down in the class with largest likelihood of post conditional (Gikunda and Jouandeau 2019).

$$P\ (C_i|X) > P\ (C_j|X) \tag{2.18}$$

for (1 <= j < i && j ≠ i). The Equation (2.18) is utilized to get Equation (2.19).

$$P\ (C_i|X) = \frac{P(X|C_i)P(C_i)}{P(X)} \tag{2.19}$$

However, to minizie the computing costs, classifier produces naive or simplistic conditions that the features n shall be independent from one another. Conditional independence of the class is expressed as Equation (2.20):

$$P\ (X|C_i)= \prod_{j=1}^{n} P(f_j|C_i) \tag{2.20}$$

Because P(X) for every class is constant and P (C i) $=\frac{|C_i|}{N}$, the NB classification can only maximise P (X|C i). Because it calculate class distribution, the computation cost is considerably reduced. Bayesian classification is simple to implement, which require single data scan to achieve highest precision (Zhang *et al.* 2019)

2.6.2 Random forest classifier

Random forest consists of h (x, _k) k = 1,2,...., Arbitration random Forest generates a tree selection. whereas Θk is scattering vectors unequally distributed and every tree chooses common category unit for the x input. A tree selection is generated using Arbitration random Forest.

If N is file size in preparation set, N files are presented separately from the original information, but by division; it is bootstrap test and Breiman used this procedure. This example served as a foundation for tree's growth. When M are the input elements, m is determined with the purpose of randomly selecting m elements in M at every location, with m units optimal distribution at centre separation. Backdrop field development evaluation of m is maintained (Zhang *et al.* 2019). As a result, several trees are generated in the backdrop forest; N determines the tree's size. The number of variables items (m) chosen in every centre is denoted in the item by the letters m, t, r, and y. The tree's dept is restricted by the size of parametes such events number in leaves and nodes, generally set as one. As described above the condition where forest is ready other events are paused utilizing all the trees that have already been planted. The new event are recorded as vote for each tree (Daghrir *et al*. 2020).

The quantity of votes are totaled from all trees, class by greatest votes, e.g., the biggest proportion of votes, is used to describe the new event. Whenever initial test kit is made by analysing and exchanging each tree and measuring its creation, around 1/3 of the examples cases are missing. (OOB) data is the name of this setting Individual mistakes are estimated using an OOB information index that is unique to each tree. It's referred to as OOB error evaluation. (Gikunda and Jouandeau 2019) describes a forest random generalisation error in Equation (2.21)

$$RE^{*} = f_{xy}\big(mg(X.Y)\big) < 0 \qquad (2.21)$$

Margin function is provided as Equation (2.22)below

$$mg(X.Y) = av_k I(h_k(x) = Y) - max_{j \neq Y} av_k (h_k(X) = j) \qquad (2.22)$$

The margin function calculates how much the average number of votes for the appropriate class at (X, Y) outnumbers the other class average vote (Han *et al.* 2011). The anticipated value of the margin function is used to determine the Random Forest's strength as shown in Equation (2.23)

$$S = E_{X.Y}\big(mg(X.Y)\big) \qquad (2.23)$$

An upper bound on generalisation error is provided by, where ρ is the mean value of the correlation between base trees, Equation (2.24)

$$PE^{*} \leq P(1 - S^{2}) / S^{2} \qquad (2.24)$$

As a result, in order to improve Random Forest accuracy, the underlying decision trees must be diversified and precise (Han *et al.* 2011).

2.7 Deep Learning

Artificial intelligence that simulates the brain functions in terms of data organisation and job completion for use in dynamics is known as Deep learning. In false intelligence, deep learning refers to networks that can absorb unstructured or unlabeled material. Deep neural learning is another name for deep neural organisation (Gobalakrishnan *et al.* 2020).

Deep learning has numerous layers of nonlinear manipulation that act similarly to organic sensory systems. An info layer, numerous hidden layers, and a spectacle layer are the fundamental components of a deep neural structure. Every inner layer utilises imaging of the preceding layer as information, and each layer has linked hubs or neurons. Deep learning is used to extract highlights from picture data and is more frequent than traditional AI methods. Deep learning architecture includes the Recurrent Neural Network (RNN), Deep Belief Network (DBN), Convolutional Neural Network (CNN), and others (Sultana and Puhan 2018).

Furthermore, because deep learning is a type of AI, it collects materials and executes tasks that are genuinely defined by images, text, or voice. The layers number in the greatest layer structure, the deepest organisation, is referred to as "deep". There are other in-depth learning approaches, such as the one discussed above, but this work focuses on the Deep Convolution Neural Network, which is the most well-known and capable of detecting and determining skin cancer (DCNN).

2.7.1 Artificial neural networks (ANN)

The non linear manipulation of neurons calculations are suppressed sophisticatedly by Natural networks. Figure 2.6 depicts the arrangement of neuronal imitation. Artificial neural organisation is commonly utilised for clinical images because it has a high prognostic intensity (Sultana and Puhan 2018).

Test pictures are supplied to neurons in an artificial global neural structure to prepare them. A backscatter algorithm is employed to prepare the neurons, with the flow forward. Generated result is then compared to the ideal result, and an mistake sign is made in the event that the two productions do not competition. The regressive route is lengthened as a result of this inaccuracy. To decrease mistakes, loads are changed. This handle is pressed again and again until the error is zero (Rey-Barroso *et al.* 2021).

In brain architecture both activation work and connecting hub form a serial structure. Sigmoid capacity, Overstated peptic volume, direct volume per component, and verge purpose are among active resources. An information layer provides information projects to the organisation, which merges with the concealed layer at this time, and output layer is interfaced with the wrapped layer, as exemplified in Figure 2.7 (Reddy *et al.* 2019).

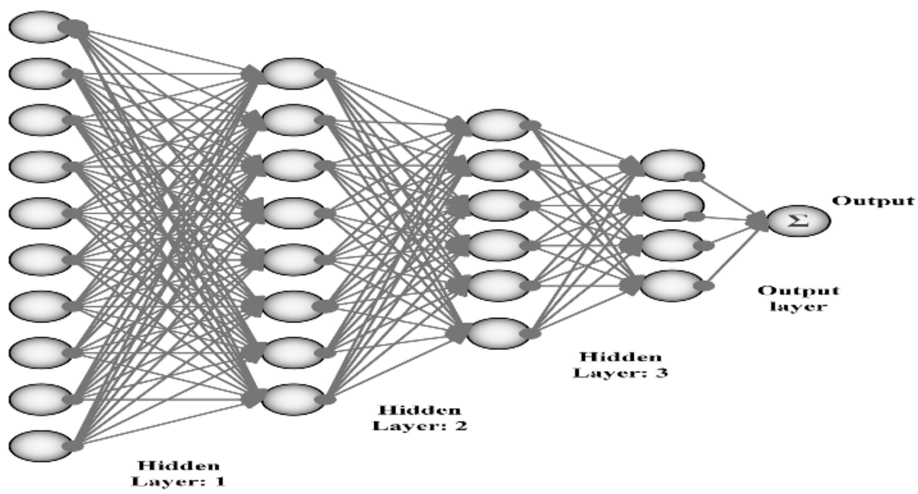

Figure 2.7 Plot of (ANNs)

2.7.2 Convolutional neural networks (CNN)

A CNN is a feed-forward artificial neural NN that contains of one or additional convolutional layers supplemented by unique or additional completely linked layers, similar to a typical Multi-Layer Perceptron (MLP) (Sultana and Puhan 2018). As depicted in Figure 2.8, a CNN is a feed-forward neural network. Without any loops or cycles, the signal is handled right here. (Reddy *et al.* 2019) Equation (2.25):

$$G(x) = gn(gn - 1\left(\ldots\left(g_1(x)\right)\right)) \tag{2.25}$$

whereas N is hidden layers total numbers, X signifies the input signal, and gn represents layer N's corresponding function. A convolutional layer in a simple CNN model is made up of g function with several convolutional kernels (h1, ... hk-1, hk) Equation (2.26). Every hk represents a linear purpose in the kth kernel, as seen in (Sultana and Puhan 2018).

$$h_k(x.y) = \sum_{s=-m}^{m} \sum_{t=-v}^{n} \sum_{v=-d}^{w} v_k(s.t.v)x(x - s.y - t.z - v) \tag{2.26}$$

where (x, y, z) shows input X pixel position, n shows width, w is the filter depth, m shows height, andv_k represents the weight of kth kernel (Zhang *et al.* 2019).

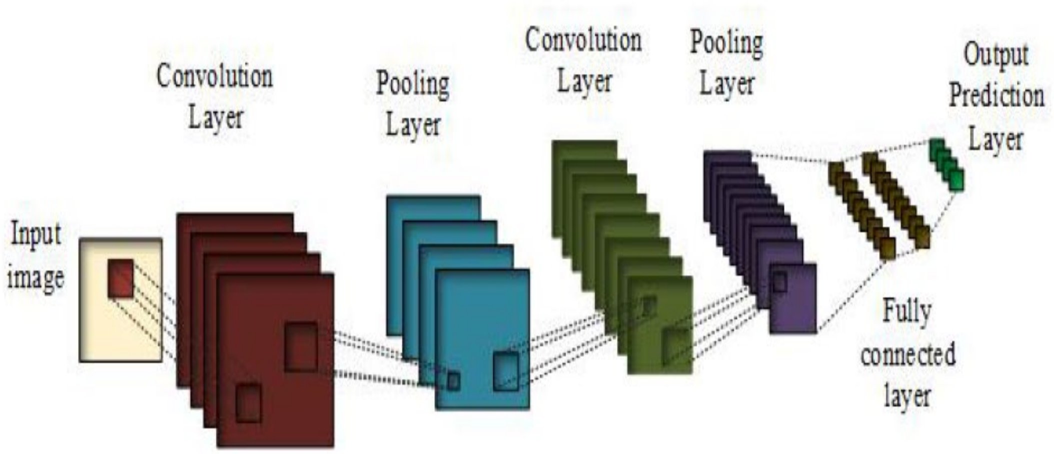

Figure 2.8 General convolutional neural networks

Downsampling is the primary purpose of CNN grouping, which relates nearby pixels and replace them in display in a region with summary features. The immutability of rotational and interpretative changes is reproduced by pooling, which lowers dimensionality and reduces dimensionality. One of the most well-known polar capabilities (Sultana and Puhan 2018) is max pooling, where area of rectangular pixels efficiency is thoroughly estimated.

The typical value of rectangle area in normal grouping mode is assumed in display. Normal weighting is another type, which is based on the right focus pixel routes. Grouping aids in the immutability of the representation for slight changes in information interpretation. Atrous Convolution is always accompanied by the following condition: The Equation (2.27) specifies Atreus Convolution (Rey-Barroso *et al.* 2021).

$$y[i] = \sum_{k=1}^{k} x[i + r.k]w[k] \tag{2.27}$$

Whereas x[i] is one-dimensional input signal, w[k] is k-length filter, and the input signal is smapled with r istride rate. y[i] is Atrous convolution output. The output y for each position I, the input x go thorugh Atrous convolution, followed by a w filter with r Atrous rate, which correlates to the stride rate (Reddy *et al.* 2019)

Deep residual learning is utilized for counteract deterioration, which happens when deep networks meet, i.e. when accuracy, depth, and degradation saturation all increase. Instead of the required basic map, the residual network permits evidently layered layers to fit in the residual map. According to test results, residual network optimization is simple, precision is attained with large increament in depth. In deep neural networks, good connections assist to transcend information (Zhang *et al.* 2019).

When you go through too many levels, you risk losing information over time know as disappearance trend. Escape interconnections offer the benefit of lower level feature information, making minute features easy to identify. Over-polling activities have resulted in the loss of some local information, but escape interconnections enable to get additional information about the final layer in terms of improving ranking accuracy (Sultana and Puhan 2018).

Different activation functions can be utilised in the activation layer (Daghrir *et al.* 2020)

(i) In Equation (2.28) the signmoid activation function is presented (Mitra and Acharya 2005)

$$\sigma(x) = \frac{1}{1+e^{-x}} \tag{2.28}$$

It is non-linear; its combining will too be result in non-linear as well, allowing to construct layers freely. On the x-axis, it has a range of -2 to 2 and is fairly vertical on t y-axis, suggesting abrupt variations in y response to tiny value variations

(ii) The advantage of activation function is that its output is in between 0 and 1

(iii) Following is the explanation for Tanh as shown in Equation (2.29) (Rey-Barroso *et al.* 2021).

$$f(x) = \tanh(x) = \frac{2}{1+e^{-2x}} - 1 \tag{2.29}$$

It is also identified as the scaled sigmoid function as shown in Equation (2.30):

$$\tanh(x) = 2sigmoid(2x) - 1 \tag{2.30}$$

It has a range of -1 to 1. The tanh function has a steeper gradient than the sigmoid function.

(iv) The most widely employed activation function is the Rectified linear unit (ReLU) (Rey-Barroso *et al.* 2021), where g indicates a nonlinear pixel-wise function. If x is positive, it produces x; otherwise, it produces 0 as shown in Equation (2.31) (Wang *et al.* 2019).

$$g(x) = mx(0.x) \tag{2.31}$$

ReLU is intrinsically nonlinear, and the resultant multiple is nonlinear as well, allowing multiple layers to be piled on top of one other. It has a range of 0 to infinity, which means it can disturbactivation. G lowers size of the characteristics in the polling layer, the bottom layer action. 1 * 1 confusional kernel is present in fully enclosed layer. A soft mix in prediction layer forecasts the likelihood of Xj belonging to a distinct class (Kumar *et al.* 2018).

2.8 Related Work

(Daghrir *et al.* 2020) provide a cross technique for noticing growth skin cancer that might be used to some suspicious lesion. The suggested approach is based on the predictions of three separate methods: CNN and two standard mechanism learning classifiers that were skilled with a collection of characteristics that describe the boundaries, texture, and colour of a skin lesion. Then, via majority vote, these strategies are integrated to increase their performance. To test and evaluate the proposed system performance, the International Skin Imaging Collaboration (ISIC) dataset has been usedand, it contains 640 images. Acording to the obtained results, it is observied that usage the three methods composed, gives the uppermost correctness level of 88.4%.

(Hudson and Cohen 2003) uses today's extremely efficient deep CNN to answer the requirement for an intelligent and speedy skin cancer categorization system. Also, they emphasis on the categorizing the skin cancer usage ECOC SVM, and deep convolutional neural network. RGB format imageries of the skin cancers are calm from KGGLE is usage to assess the future system performance. Noises such as various organs and tools can be originate in certain of the collected photographs. For better results, these photos have been collected to remove noise. The answers were acquired by consecutively a optional procedure on 3753 photos, which comprised four dissimilar kinds of skin malignancies. The implementation result reveals the optimum accuracy mean to be 95.1%.

In (Zhang *et al.* 2019, Hu *et al.* 2018), a meta-heuristic optimised CNN classifier to classify skin cancer images using pre-trained network models for visual datasets. However, there are a variety of approaches for optimising neural network learning strategies, and there are only a few research on deep learning-based neural networks and their applications. The weight and biases in CNN models are optimised using a new strategy based on the whale optimization algorithm in this paper. On two skin cancer datasets, namely DermI S Digital Database and Dermquest Database, the novel technique is compared against ten popular classifiers. The adoption of this improved approach outperforms previous categorization methods in terms of accuracy, with a 91 percent accuracy rate.

In literature (Kumar *et al.* 2018) an better technique for early detection of three types of skin malignancies has been presented. The careful contribution is a skin lesion picture, which the system would categorise as malignant or non-cancerous using the suggested approach. To distinguish homogenous picture areas, fuzzy C-means gathering is usage for image segmentation. The picture properties are enhanced using various filters, while the other aspects are analysed using a combination of rgb color-space, Local Binary Pattern (LBP), and GLCM algorithms. Furthermore, the artificial neural network (ANN) is skilled usage the differential evolution (DE) technique for classification. Using the HAM10000 and PH2 skin cancer picture datasets, several attributes are precisely approximated to produce superior outcomes. The simulation results suggest that the proposed approach effectively identifies skin cancer with a 97.4 percent accuracy.

In literature of (Boman and Volminger 2018), made an effort to adopt the Stanford report's strategy and analyse the CNN's effectiveness during categorization of skin lesion assessments that were not investigated in their study. Melanoma vs solar lentigo and melanoma versus seborrheic keratosis are two previously unknown binary classification use cases. Inception v3 was trained for diverse skin lesions using transfer learning. A total of 16 training classes were used to prepare the CNN. During the CNN's evaluation, a 3-way classification attained an accuracy of 68.3 percent. With the same comparisons as the Stanford study, melanoma against nevus had a 71 percent accuracy rate, while seborrheic keratosis versus basal and squamous cell carcinoma had a 91 percent accuracy rate. For seborrheic keratosis vs melanoma, the accuracy rate was 84 percent, and for solar lentigo versus melanoma, it was 83 percent.

(Kaur and Jindal 2016), provide an efficant system for discovery and dignosis of skin cancer usage images and meta-data. ISIC 2019 dataset was usage to test and assess the presentation of the propsed system. Despite the fact that the dataset covers nine classes, one of them is an outlier and is not included. To address the problem, we employ an ensemble of classifiers that includes 13 convolutional neural networks (CNNs), two ways for dealing with outliers, and a simple method for using meta-data with pictures. The findings achieved are consistent with the prior challenges, and the methods for detecting the outlier class and dealing with meta-data appear to be effective. The suggested approach produced good results, with a 91 percent accuracy rate.

2.9 Evaluation Methods

The performance of diagnosis and detection systems is assessed using evaluation measures that are both quantitative and qualitative. In many cases, test scenarios are created that are based on specific assessment criteria and metrics. This section discusses assessment metrics in relation to various features and evaluative purposes

The confusion matrix is visualisation tool that is commonly utilize to examine the precision of classifiers in classification (Kaushik *et al.* 2014). This tool is being used to describe the connection amid the real and predictable classes. The misperception matrix is utilize for calculating the competence level of organization model, which is determined by categorising the right and wrong number of classifications in each variable. For a two-class classifier (Boman and Volminger 2018), Table 2.1 displays the confusion matrix:

Table 2.1 Two classes confusion matrix

Confusion Matrix		**Predicted**	
		Negative	**Positive**
Actual	Negative	TN	FP
	Positive	FN	TP

TP and TN are abbreviation for True Negative and True Positive, and include the positive and negative state proportions that were accuractely categorised (Gikunda and Jouandeau 2019). Furthermore, FP is for False Positive, reffering to negative instances classified as positive wrongly, and FN shows False Negative, referring to all positive cases that were erroneously secret as negative (Sultana and Puhan 2018). In this work, the most common evaluation methods which are accuracy, sensitivity, and specificity have been used and it is presented below:

2.9.1 Accuracy

The most typical criterion for evaluating the proposed system performance is accuracy. It assesses the classifier's capacity to deliver high-quality diagnoses (Munir *et al.* 2019, Santra and Christy 2012). The accuracy formula is shown in Equation (2.32).

$$\text{Accuracy} = \left(\frac{\text{TP}+\text{TN}}{\text{TP}+\text{TN}+\text{FP}+\text{FN}}\right)*100 \tag{2.32}$$

2.9.2 Precision

Accuracy is a computer science term that focuses on data security, information retrieval, and image processing (Nahata and Singh 2020). It is decided to put the suggested system to the test. Furthermore, accuracy is a requirement that is determined by looking at the total number of outcomes. While looking up the total number of results (Patil and Patil 2012). It's easy to figure out using the Equation (2.33) below:

$$\text{Precision}=\frac{\textbf{TP}}{\textbf{TP}+\textbf{FP}} \tag{2.33}$$

2.9.3 Recall

The classifier's ability to recognise the right positive samples is measured by recall. A True Positive Rate (Munir *et al.* 2019) is another name for it. Equation gives the recall Equation (2.34)

$$\text{Sensitivity} = \left(\frac{\text{TP}}{\text{TP+FN}}\right) \tag{2.34}$$

3 RESEARCH METHODOLOGY

3.1 Introduction

In most nations, skin cancer is the most frequent malignancy, with melanoma accounting for the bulk of skin cancer-related fatalities. Many deep learning-based algorithms for categorising photos of skin cancers, both benign and malignant, have been created in recent years. According to some accounts, their precision was on par with, if not better than, dermatologists'. This chapter outlines the design and implementation of the proposed system, as well as the methodologies and algorithms employed.

3.2 The Proposed System Discretion

In the current research work, Autonamous Skin Cancer detection and diagnosis System has been proposed, it is on deep learning basis by employed the Deep Convolutional Neural Network (CNN) and machine learning by employed the Random Forest, and Naive Bayes. The proposed sysem has the ability to detect and diagnose Skin cancer in early stage. Proposed system building is presented in Figure 3.1

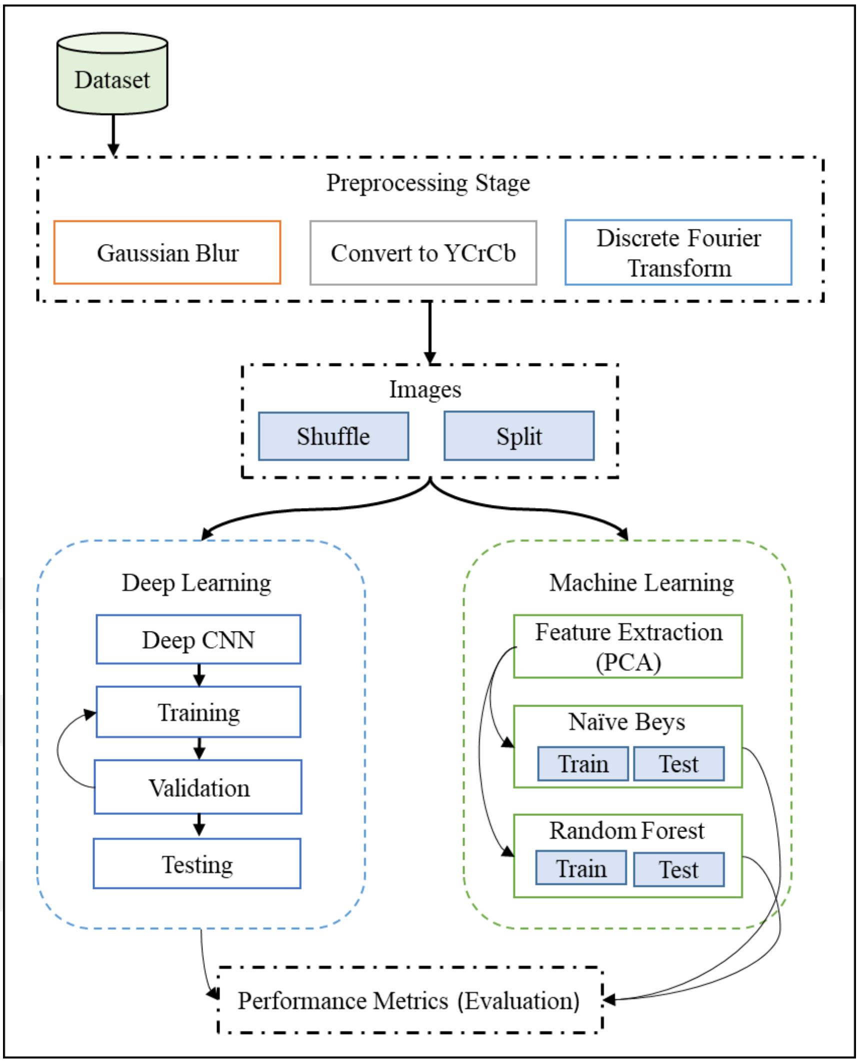

Figure 3.1 General block diagram of the proposed DPD-DCNN

The proposed DPD-DCNN system includes five primary steps, as indicated in Figure 3.1. (from the dataset loading leaf image, accuracy performance splitting and shuffling dataset, pre-processing image, Deep learning basis classification, finally, machine learning). Each primary step of the proposed system contains sub-stages, all of which work together to meet the proposed system's aims, as shown in the paragraph below.

3.3 Testing Dataset and Input images

To evaluate and test the proposed system performance, the International Skin Imaging Collaboration (ISIC) has been used. It's a collaboration between academics and business aimed at making it easier to use digital skin imaging to help lessen cancer mortality. Melanoma is easily curable if noticed and treated in its early stages. Through tele-dermatology, clinical decision support, and automatic analysis, digital photographs of skin lesions may be utilised to teach specialists and the general public about melanoma detection as well as straight help in the analysis of melanoma. ISIC seeks to fulfil its objectives through developing and promoting digital skin imaging standards, as well as collaborating with dermatology and computer science to enhance diagnosis. ISIC is working on suggested standards to improve digital skin image quality, privacy, and interoperability (the aptitude to share pictures across different technological and clinical platforms).

ISIC is creating resources for the dermatology and computer science communities, including a large and expanding open supply public get right of entry to archive of pores and skin pics desires. This archive serves as a public useful resource of pics for teaching, research, and for the development and trying out of diagnostic artificial intelligence algorithms. ISIC is engaging the stakeholder communities through meetings, publications, conferences, and the hosting of artificial intelligence Grand Challenges. In this work, the data contains 3297 images and two classes which are benign and malignant in different cases. The dataset is orgenaly segmeanted in two trainaing and testing. Furthermore, a total of 2637 images is used for training and a total of 660 images have been used for testing and evaluatiog the presentation of the proposed system. Moreover, the sample of Melanoma and Benign cells are depicted in Figure 3.2.

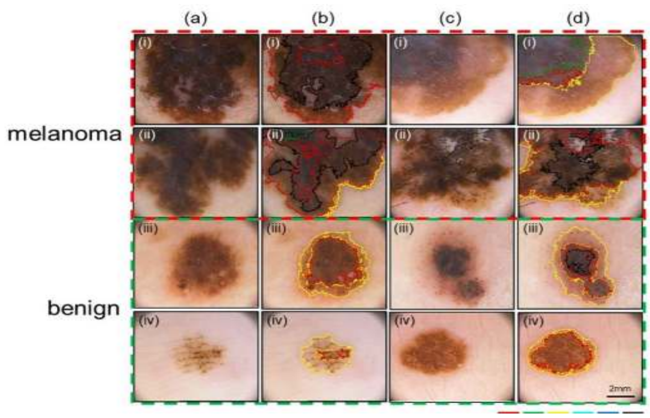

Figure 3.2 Sample of Melanoma and Benign cells in different cases(Kumar *et al.* 2018)

Morever, the feasibility of this work is demonstrated by deep learning and machine learning approaches to enable automatic disease diagnosis through image recognition. All of these images are available in RGB arrangement and have a resolve of (256 * 256) pixels. Basically, the ISIC dataset was chosen because it free and online available and it has the attributes of the skin cancer which were used in this work:

3.4 The Proposed System

Preprocessing, shuffling, and splitting Images and classification phases are the three stages of the proposed system, which are detailed below:

3.4.1 Preprocessing stage

The second stage in the Proposed system is preprocessing which is an important process and its first stage in the classification system that was used before the application of any type of classification technique. The dataset is containing a number of images, these images may obtain noise, shadow, and unimportant detail. This may result in misguiding results. As a result, before working on a study, preprocessing seeks to reduce noise and recognised regions of interest (ROI). This stage is divided into four major secondary stages, as indicated in Figure 3.3

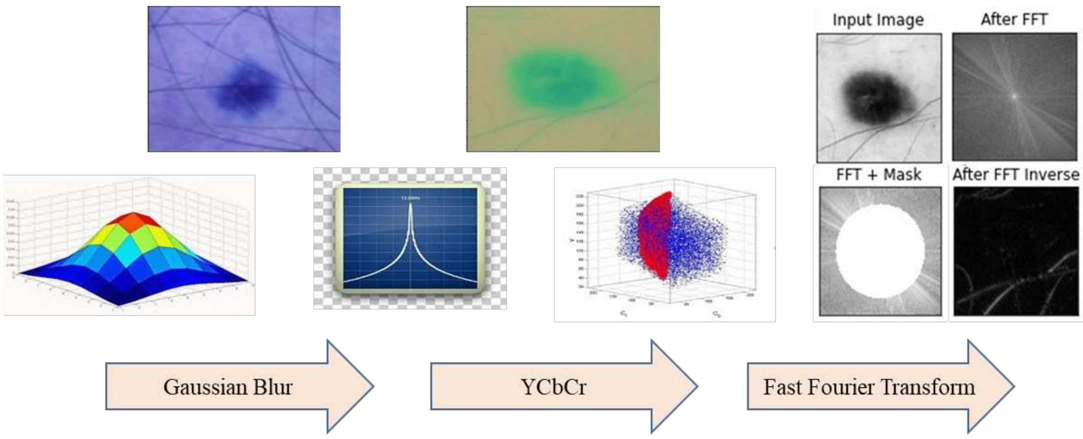

Figure 3.3 The preprocessing stage

3.4.1.1 Fastest gaussian blur

The goal of employing the quickest Gaussian blur filter is to reduce noise from the input photos so that a Gaussian function can blur the image When blurring a picture, the colour change from one lateral of an image's edge to the additional will be flat somewhat than sudden. Fast variations in pixel strength are be around out as a consequence of this result.

A convolution procedure amid the input picture and a Gauss filter kernel is what Gausian blur. The specifics of the quickest Gaussian blur are shown in Algorithm 3.1, where the algorithm's inputs are left pictures and the radius depicts "sigma" or "standard deviation". 2D functions is denoted as matrices of values throughout this approach, and the weight will be referred to as the kernel. The weighted average of the density function around [i, j] multiplied by weight is the value of convolution at [i, j]. The outcome of the quickest Gaussian blur stage is shown in Figure 3.4

```
Algorithm(3.1)   Fastest Gaussian Blur
Input: image  , radius
Output: imagGaussian Blur
Begin
Step 1: significant radius
        rs = radius* 2.57
Step 2
    For each (i=0,j=0;i<  h, j<w; i++, j++)
    val = 0, wsum = 0
    For each (iy= i-rs, ix = j-rs; iy<i+rs+1, ix<j+rs+1; iy++, ix++)
        x= Min(w-1, max(0, ix) )
        y= Min( h-1, max(0, iy) )
        dsq = (ix-j)*(ix-j) + (iy-i)*(iy-i)
        wght = Exp( -dsq / 2r² )/ ( 2r² PI)
        val += image (y*w + x) * wght
        wsum += Wght;
     End for
    imagGaussian Blur [i, j] = val/wsum;
End for
```

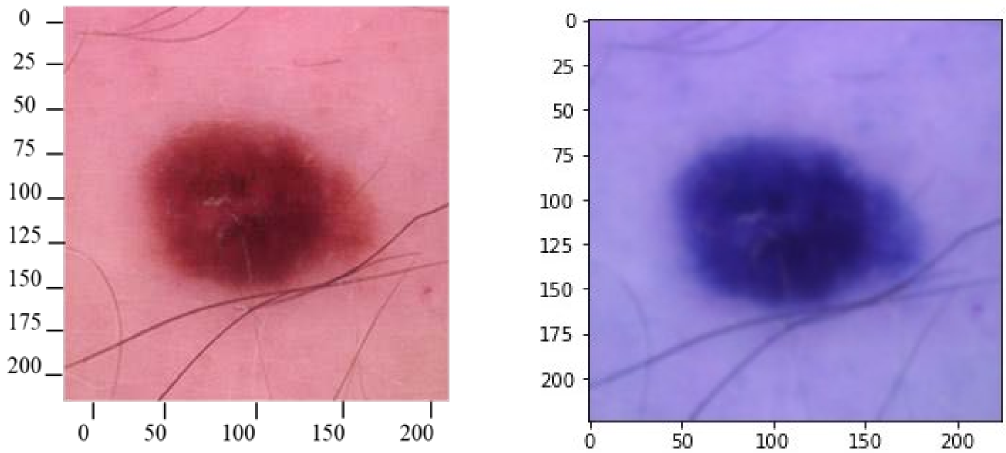

a) Original Image b) Gaussian Blur image

Figure 3.4 Fastest Gaussian blur algorithm example

3.4.1.1.1 Convertion from RGB to YCbCr color space

After applying the result of the quickest Gaussian blur to the RGB colour picture of the dataset, transform the colour space of the images to YCbCr to produce ROI (diseases area) in infected and healthy images more visible. The chrominance and luminance of the image is distinguished in YCbCr. Image's brightness will be saved in the Y-channel. As demonstrated in Algorithm 3.2, the Cr and Cb channels store chrominance in red and blue directions Also displayed is an example of converting a colour picture from RGB to Ycbcr colour space in Figure 3.5

Algorithm(3.2) convert color image from RGB to YcbCr
Input: RGB imagGaussian Blur
Output: Ycbcr image
Step 1: For each pixel (R,G,B) in imagGaussian Blur

$$Y=0.299R+0.587G+0.114B \quad (3.1)$$
$$Cr=-0.169R+0.331G+0.5B \quad (3.2)$$
$$Cb=0.5R-0.419G-0.81B \quad (3.3)$$

End for
Return image
End

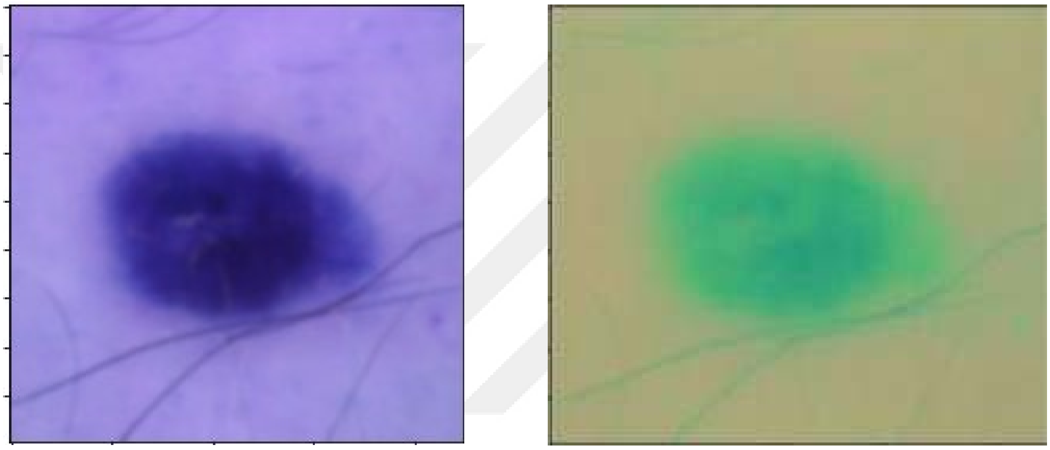

a) Gaussian Blur b) YCbCr image

Figure 3.5 Convert color image from Gaussian to Ycbcr example

The green component has the greatest influence on the Y-channel, as shown in Figure 3.5, since natural eyes feel green first, following red then blue color components. When R, G, and B are all in the 0-255 range (as in 24-digit pictures), Y is likewise in the 0-255 range, while Cb and Cr have ranges of – 128-127. The value 128 is commonly attached to channels Cb and Cr to brand them share of an nameless byte info kind.

3.4.1.1.2 Fast Fourier Transform

The image application channel in iteration area is quicker then image execution space hence the fourier converstion is fast, FFT is used to bringing image to iteration area from spatial image space. In the Algorithm 3.3 it is clearly illustrated by applying FFT algorithm to Ycbcr image. The frequency domain forward and back is required for forward and inverse transformation. (Figure 3.6)

Algorithm(3.3) Fast Fourier Transform
Input: Ycbcr image
Output: Grayscale image
Step 1: Compute the 2-dimensional Fast Fourier Transform
Step 2:Shift the zero-frequency component to the center of the spectrum
Step 3: Inverse of Step 2. Shift the zero-frequency component back to
original location
Step 4: Inverse of Step 1. Compute the 2-dimensional inverse Fast Fourier
Transform.

Figure 3.6 Algorithm 3.3 fast fourier transform (FFT)

The FFT steps stated in Algorithm 3.3 are implemented to an anthracnose image, as shown in Figure 3.7. The sign decomposes into fragmented sections, resulting in its frequencies. The image goes from space region to reproduction area at the conclusion of the FFT. Each point in the first figure refers to a certain repeat. Following FFT, picture is altered so that DC segment F (0, 0), represents brightness, is presented in the image's centre.

In furthermore, the high iteration intensity is seen in the white part of the interval picture in Figure 3.7 which is exhibited after the FFT. Low frequency ranges are shown in the image's corners. As a result of combining two points, the white region at the angle has a lot of energy at low / zero frequencies, which is a frequent occurrence in most photographs.

The interpretation and inversion capabilities of the FFT Cover 2-D FFT shown in Figure 3.7 allow it to be relocated without losing data pieces. The area's picture is made more apparent to humans by moving the zero-repetition section to the centre. Furthermore, this interpretation can assist us in smoothly operating the High/Low Pass channel. Next, the inverse Fourier Transform was used to create the first image without low frequencies, as shown in Figure 3.7.

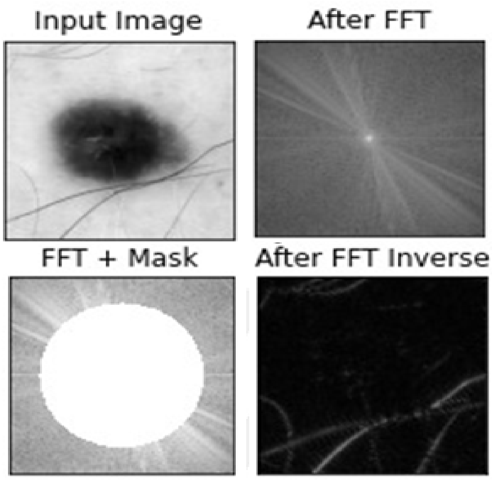

Figure 3.7 Fast fourier transform (FFT) steps

The morphological Gray dilation operation is the final stage in the preprocessing procedure. Because the Gray image obtained in the previous step contains both strong and weak pixels. This step focuses on making weak pixels extra apparent, fill in tiny holes in objects, and eliminate regions on the resulting image that are considered unimportant areas or noise. While keeping the beneficial areas for computation in the following steps. By adding pixels to the image pixels, a dilation operation widens the picture pixels and extends the object bounds. Furthermore, the outcome pixel value is equal to the sum of all neighbouring pixels' maximum values. The dilation procedure is depicted in full in Algorithm 3.4 (Figure 3.8)

Algorithm (3.4) Morphology Dilation Operation

Input: Grayscale image, Kenel= $\begin{bmatrix} 255 & 255 & 255 \\ 255 & 255 & 255 \\ 255 & 255 & 255 \end{bmatrix}$

Output: output Grayscale image

Begin

Step 1: for all pixel in image do

Step2 :if pixel = 255 then

Step2-1:get all neighborhood in pixels

Step2-2:Comparison between kernel and neighborhood pixel if

deferent replace with value kernel

Step3 :else

Step3-1:Loop

Step4:end if

End

Figure 3.8 Algorithm 3.4 morphology dilation operation

Algorithm 3.4 require two inputs in dilation operation. The initial is the dilated component of an image in (grey) format. The second is a structural element, which is a (typically tiny) group of coordinate points (the kernel). On an anthracnose-infected leaf picture, Figure 3.8 illustrates an example of the result of the morphological Gray dilation procedure.

3.4.2 Splitting and shuffling images stage

The proposed system is divided in two subsystem as discussed in previous chapters. First subsystem relies on machine learning, whereas second one relies on deep learning. Moreover, because the dataset is sorted by class there is a need for shuffling in the case of machine learning. Whereas, in the case of deep learning there is a need to split the dataset into training and testing to evaluate the obtained results and then compare with the related work. The first part of dataset segemented constitute 70% for training in data set for proposed system. While, second part constitute 30% for testing the proposed system performance. This segmentation has been done according to the related work which they compared with our proposed model. The dataset was shuffled and divided as described below in order to produce the Gray pictures.

i. Shuffling dataset: Python's "random. Shuffled" function was used to reorder the data. This is an arbitrary number generator-based computational rearrangement request. Following application, the picture query is mingled with the full database, which was previously in sequential order.

ii. Splitting dataset: The associated project make a data set; the first 30% of whole dataset is presented as test set, followed by the rest of the data in a 70/30 pattern. The remaining funds will be utilised to train the algorithm. The algorithm is prepared using the preparation and approval sets.

3.4.3 Classification stage

The system proposed is composed of two parts in the classification stage:1) Utilizing CNN method for deep learning. 2) and second is machine learing alongwith two subset: Utilizing PCA algorithm for feature extraction and using (Random Fours, and Nave Bayes) algorithms for classification.

3.4.3.1 Deep learning using CNN algorithm

This dataset contains photos that are either healthy or ill and are labelled Melanoma, Benign and Healthy. Images were split into training 70% and 30% for testing. In Algorithm 3.5 the CNN algorithm is used to demonstrate the classification step in detail. Moreover, these validation, training, and testing percentages have been adjusted in accordance with the associated work outlined in the preceding chapters (Figure 3.9)

```
Algorithm (3.5) CNN algorithm
Input: Training data
Output: CNN Mode
Begin
Step 1: Training data set
Step 2: Create layers mode
        Step2-1:Convolutinal2D(Conv =16,Size Mask=(3, 3,) activation='relu')
        Step2-2:,MaxPooling2D(pool_size -(2, 2)
        Step2-3:Convolutinal2D(Conv =32,Size Mask=(3, 3,) activation='relu')
        Step2-4:,MaxPooling2D(pool_size = (2, 2)
        Step2-5:Convolutinal2D(Conv =64,Size Mask=(3, 3,) activation='relu')
        Step2-6:,MaxPooling2 D(pool_size = (2, 2)
        Step2-7:Convolutinal2D(Conv =128,Size Mask=(3, 3,) activation='relu')
        Step2-8,MaxPooling2D(pool_size = (2, 2)
        Step2-9:Convolutinal2D(Conv =512,Size Mask=(3, 3,) activation='relu')
        Step2-10.,MaxPooling2 D(pool_size = (2, 2)
        Step2-11:Convolutinal2 D(Conv =1024,Size Mask=(3, 3,) activation='relu')
        Step2-12:,MaxPooling2D(pool_size = (2, 2)
        Step2-13 Flatten
        Step2-14:, Dropout(0.6)
        Step2-15:, Dense(0.6)
        Step2-16., Dense (1024, activation='relu'
                        ,kernel_regularizer=regularizers.l2(0.002)
        Step2-17: Dense(14, activation= 'softmax'))
Step3 :Error J(W) Calculation Back Propagation Parameter update
         If Convergence =no then
             Epoch +=1;
              got step 1
          Else
           Got to step 4
Step : save CNN Mode
End
```

Figure 3.9 Algorithm 3.5 the CNN algorithm

CNN deliver final calss by passing a raw image through network layers as depicted in Algorithm 3.5. A feature map in the CNN technique comprises of several layers difficulty is performend on contribution infected leaf images with assistance of kernel of filter. Slide the filter with size 3*3 over ill leaf copy in the convolution layer to perform a convolution. A matrix multiplication is done at each point, and the result is summed in the feature map, as illustrated in Figure 3.10

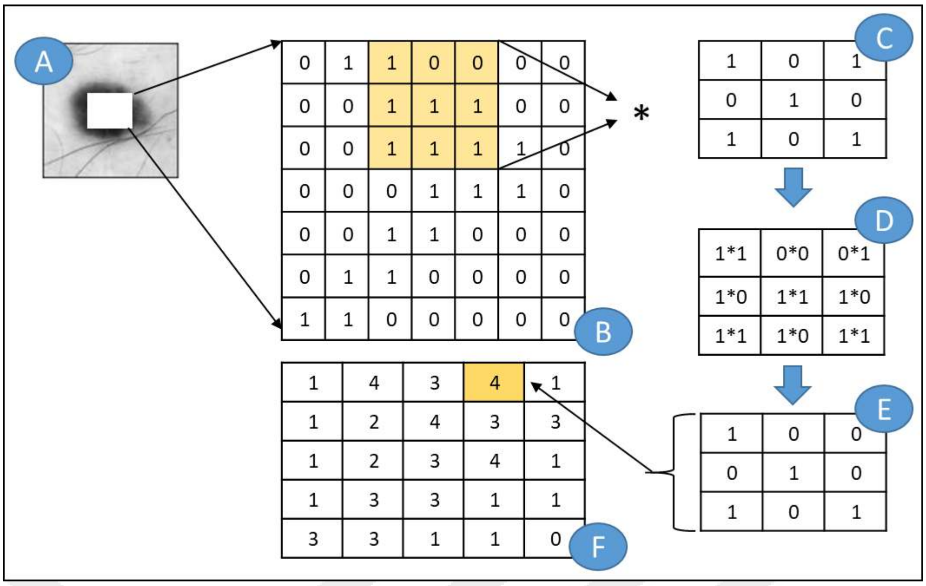

Figure 3.10 Convolutional Layer; a) anthracnose-infected Grayscale leaf image, b) input image data, c) kernel 3*3; d) data block 3*3 multiplication of kernel and input image, e) multiply operation results, e) feature map (Boman and Volminger, 2018)

Morever, in Algorithm 3.5, the activation function is introduced to our network somewhere among 2 convolutional layers or at the network's end. It assists in deciding which data should be forwarded and what should not to made judgments at the network's end. It's used a lot and does its job well; it's a probabilistic technique to making decisions with ranges between 0 and 1, so it's best to use this activation function when you need to come to a decision or anticipate an output since this range is the smallest, so the prediction will be more precise. The Rectified Linear Unit (ReLU) Activation function currently employs an start purpose that spans 0 to infinity. All negative numbers are transformed to a value of zero.

To improve processing time, the max pooling layer is employed to lower the the feature map dimensionality. Take a filter of size f*f and apply the maximum operation over the f*f sized section of the picture in the max pooling layer. Pooling is usually done using a filter of size 2*2 with a stride of 2, and the picture size is then cut in half, as illustrated in example Figure 3.11

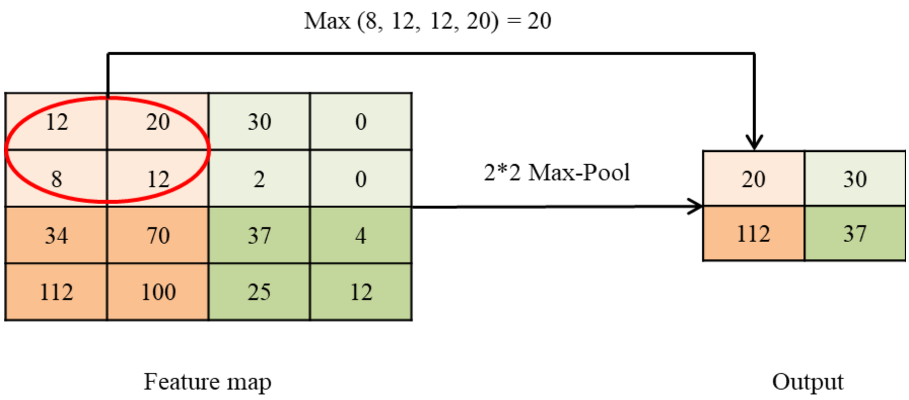

Figure 3.11 Max pool layer (Boman and Volminger 2018)

To make this one-dimensional, utilise the **flat layer**. The tensor flow framework is used for this purpose. It takes the output of preceding convolutional layers and crushes it to form a solitary property course that may be usage in classification by a fully integrated layer.

Dropout Layer deactivates or drops out input items that have a specific probability, allowing individual neurons to learn traits that are less dependent on their environment. Only during the training phase does this happen.

The usual deeply linked neural community layer is the Dense layer. It's the most popular and often utilised layer. On the input, the Dense layer performs the subsequent operation and returns the result. The only true network layer with this method is dense. In a Dense level, all the previous layer's outputs are introduced to all of the neurons, with every neuron giving one output to the subsequent layer. This is the most basic layer in neural networks.

3.4.3.2 Machine learning

Machine learning methods have been used in the further branch of classification, which comprises of 2 sub-stages (Function extraction and classification stage utilising machine learning techniques), as detailed below:

i. Principal Component Analysis (PCA)

Principal component analysis (PCA) is a statistical approach for data dimension reduction or data decorrelation that is commonly employed in signal processing. In this stage, to use the PCA algorithm, features extracted from anthracnose-infected leaf images. The selection of attributes denotes the columns number in every image; i.e., if dimension of input image is 255*255, the number of attributes equals 255, and the class number equals the input image number. Then, using the PCA technique, generate the highest eigenvectors using all class probabilities, as demonstrated in Algorithm 3.6.

Algorithm (3:6): PCA Steps
Input: number of features, Y= Number of class, K = Dimension reduction space Output: Features that have the highest contrast
Begin Step 1: Compute the mean vectors for the different classes from the dataset $\mathbf{u} = \frac{1}{m}\sum_{i=1}^{m} x_i$ (3.4) Step 2: Computing the scatter matrices 2.1: Within-class scatter matrix Sw $S_w = \sum_i^c s_i$ (3.5) $S_i = \sum_{xeD}^{n}(\mathrm{x} - m_i)\ (\mathrm{x} - m_i)\mathrm{T}$ (3.6) 2.2: Between-class scatter matrix SB $S_B = \sum_{xeD}^{n} N_i (m_i - \mathrm{m})\ (m_i - \mathrm{m})\mathrm{T}$ (3.7) Where m is the overall mean, mi is sample mean, and N is the sixes of respective classes Step 3: Compute the eigenvectors (e1, e2, …, ed) and corresponding eigenvalue (ʎ1, ʎ2…, ʎd) for the scatter matrices, Av=ʎv (3.8) and A= $\sum_w^{-1} S_B$, V=Eigenvector, ʎ=Eigenvalue Step 4: Sort the eigenvectors by decreasing eigenvalue and chose k eigenvalue with the largest eigenvalue to form a d x dimensional matrix W (where every column represents an eigenvector) Step 5: Calculate the eigenvalue for C= [ʎ1 > ʎ2, …, ʎn] Step 6: Use this d x k eigenvector matrix to transform the samples into new subspace. This can be summarized by the matrix multiplication Y=X * W (3.9) Where x is an n * d dimensional matrix representing the n samples, and Y is the transformed n * k-Dimensional

Figure 3.12 Algorithm 3.6 PCA steps

ii. Classification Stage by using Machine learning Algorithms

The suggested system's last stage is classification, and two classification algorithms have been applied in this stage: Naive Bayesian Classifier (NB) as shown in sub-section (a) and Random Force as explained in sub-section (b).

a) Naive Bayesian Classifier (NB) algorithm

A Nave Bayes classifier is a straightforward probabilistic feature model based on Bayes' theorem and the assumption of strong independence on a class feature (Tiwari *et al.* 2013) The probabilistic model is referred to as a "independent feature model" here, and the prefix nave is derived from the word "strong". The term "independence" refers to the fact that each attribute of a class contributes independently to the likelihood of a certain item being categorised. Simply said, the presence of one class feature has no bearing, under any circumstances, on the existence of any other characteristic, given the class variables. These sorts of classifiers have been shown to perform relatively better in many challenging real-world contexts (Chandel and Gupta 2013) despite their assumptions and naive design.

In many practical applications, Nave Bayes models employ the maximum likelihood approach to estimate the precise standards of the nasty and alteration as model limits to make the experiential answers the greatest likely, assumed the model. In general, the maximum likelihood technique is used to choose model parameters in order to maximise the likelihood purpose amid the selected models and the observed data, as demonstrated in Algorithm 3.7 (Figure 3.13)

Algorithm(3.7): Naive Bayes
Input: Matrix Data set
Output: Calculate the probabilities of predicting each class
Begin
Step 1: Split the dataset by class values
Step 2: Split dataset by class then calculate statistics for each row
Step 2-1: Calculate the mean of a list of class
Step 2-3 Calculate the standard deviation of a list of numbers
Step 2-4: Calculate the mean, stdev and count for each column in a dataset
Step 3: Calculate the probabilities of predicting each class for a given row
Step 3-1 Calculate the Gaussian probability distribution function for x

Figure 3.13 Algorithm 3.7 Naive Bayes

b) Random Force classification algorithm

It's a classification algorithm that employs numerous decision trees, each of which has portions that designate class tags and twigs that signify feature mixtures that principal to those tags. The training decision trees are then used to categorise untrained data in a randomised method (hence the name Random Forest), in an attempt to address the overfitting characteristic of decision trees.

The Random Force classifier was used to divide the dataset into two halves in the suggested system. The first component of the dataset covers 70% of the total dataset and is used to train the suggested system. The second half of the dataset covers 30% of the dataset and is utilised to test the proposed system, as well as to assess the suggested system's performance classification precision Skin diseases as stated in an Algorithm 3.8 (Figure 3.14).

Algorithm(3.8) Random Force
Input: Matrix Data set
Output: best tree
Begin
Step 1: Select random samples from a given dataset.
Step 2: Construct a decision tree for each sample and get a prediction result from
each decision tree.
Step 2.1: Calculate the Prior Entropy of the Data Set
Step 2.2: Calculate the Information Gain for Each Attribute
Step 2.3: Calculate the Attribute that Had the Maximum Information Gain
Step 2.4: Partition the Data Set Based on the Values of the Attribute that Had the
Maximum Information Gain
Step 2.5: Repeat Steps 1-4 for Each Branch of the Tree Using the Relevant Partition
Step 3: voting will be performed for every predicted result.

Figure 3.14 Algorithm 3.8 random force

4 IMPLEMENTATION AND EXPERIMENTAL RESULTS

4.1 Introduction

The skin have different kind of diseases, the most coomon and dangers is skin cancer. Therefore, an early and accurate skin cancer Detection and diagnosis system is required. An automatic system of proposed research work for early detection and diagnosis of Skin disease on Deep learning and machine learning basis. The system is made up of two primary subsystems, first of which is on machine learning basis and second of which is focused on deep learning, which is actual contribution of this research work. Subsequently, in this chapter, a set of experiments are conducted to test the hypothesis and determine if it is efficient to detect and diagnose the Skin cancer disease.

The experimental setting includes the use of International Skin Imaging Collaboration (ISIC) dataset which is significant for evaluating techniques performance that is employed for skin cancer detection and diagnosis. Eventually, performance metrics are applied to the described experiments in which the metrics are used to evaluate the proposed model in the simulated environment. Finally, this chapter examines the extracted outcomes as well as the experimental findings.

4.2 Implementation Environment

This section discusses the implementation environment, which is separated into two parts: software and hardware.

- **Software**: Python and Windows 10 were used in this study. Python also has a large number of libraries, classes, and functions to choose from. However, because the envisioned system environment was fully supported, this study primarily leveraged the Graphic User Interface (GUI) library to develop the simulation. Displaying pictures, simple manipulations like flipping, cropping, rotating, etc., Classification, Image Segmentation, and feature extractions, Image recognition, and Image restoration, are all included in python. Python proves to be an excellent choice for image processing jobs. This is due to its rising appeal as a scientific programming language and the ecosystem's open availability of numerous cutting-edge image processing tools.

- **Hardware**: The simulation is run on a single laptop with an Intel (R) Core (TM) i7-5500U CPU running at 2.40GHz and 16 GB of RAM.

4.3 Performance of the Proposed System

The system proposed is comprised of two subsystems, each of which uses different classification algorithms but follows the same data pre - processing dataset steps. The first system includes prognosis skin cancer disease machine learning - based using nave Bayesian and Random forest classification algorithms. While the second system represents diagnosis skin cancer disease based on deep learning using deep Convolutional Neural network (CNN). Finally, based on accuracy measures, we analysed the findings of both systems to determine which subsystem performed best in diagnosing Skin disease. As a result, the outcomes of each stage of the proposed system are shown in the subsections below.

4.3.1 Load images

The suggested system's initial step is to import photos from the ISIC dataset. As indicated in table 4.1 the dataset has two distinct classifications

Table 4.1 Skin dataset classes

#	Class	Label
1	Malignant	C1
2	Benign	C2

In addition, because the dataset is so large, each class has had five photos sampled. The picture examples for each class were shown in Figure 4.1, along with their histograms. The histogram is significant in this case because it shows the pixel distribution in the original picture so that the effects of the procedures that will be conducted on the database images in each class can be determined by comparing the outcomes of each operation to the original histogram. Moreover, the sample of inputed images for two classes is shown in Table 4.2, the Benign represents C1 and Malignant represents C2.

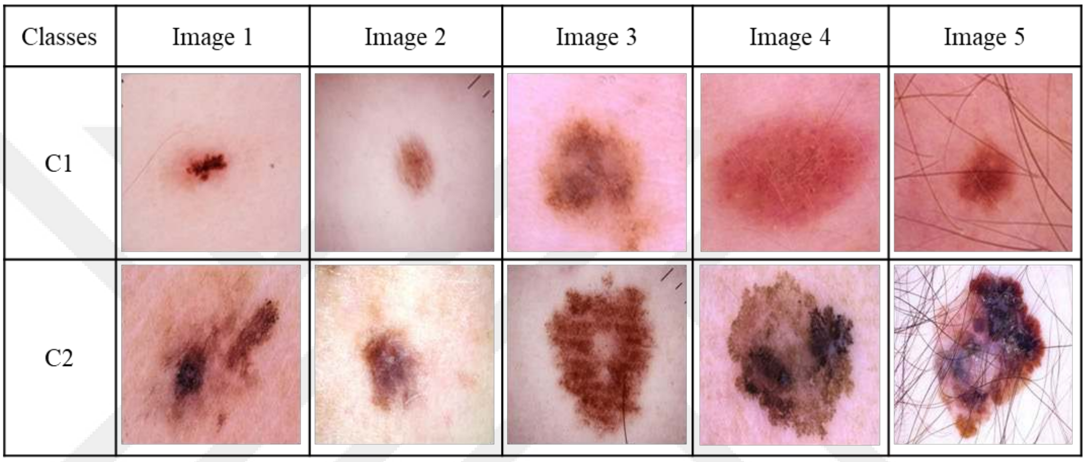

Figure 4.1 Sample of Benign and Malignant cells images

4.3.2 Images preprocessing stage results

The preprocessing stage for skin cancer images contains four sub-steps: (Gaussian Fourier, Discrete Fourier Transform, convert image from RGB to YCrCb and Morphology operation).

4.3.2.1 Gaussian results

The initial stage in image processing is remove the noice, Gaussian blur is employed in this work for this reason. However, it is applied the median value to the central pixel within a kernel size (x × y) to remove the noise which detected in the input samples of skin cancer images for each two classes as shown in the bellow table. Also, the bellow table shows the effect of Gaussian filter for the selected sample, and how to make a normal distribution of picture pixel values by smoothing out part of the unpredictability and removing all the unnecessary features (Table 4.2)

Table 4.2 Results of Gaussian Blur for skin cancer image sample with its histogram.

Class	Gaussian Blur (Benign)	Histogram	Gaussian Blur (Malignant)	Histogram
C1	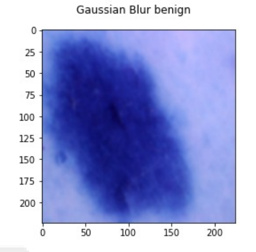	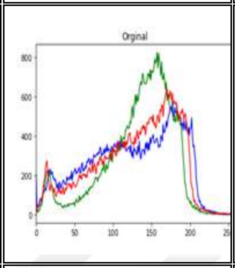	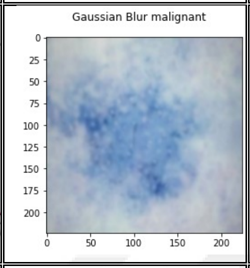	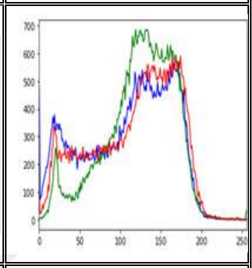
	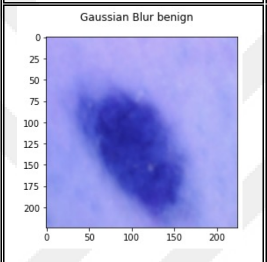	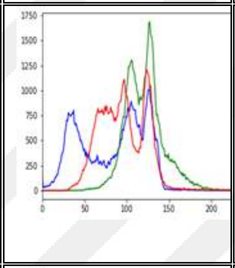	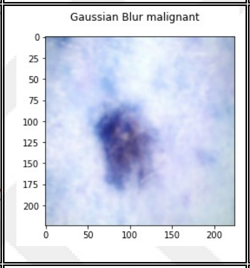	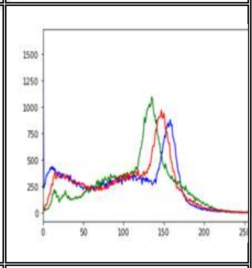
	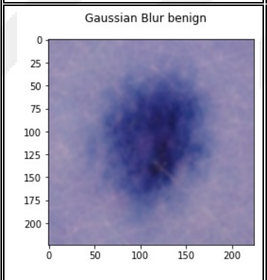	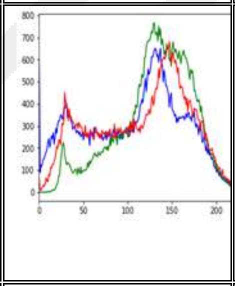	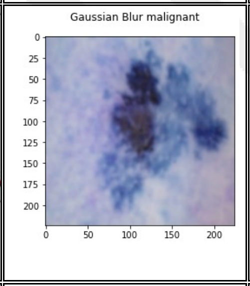	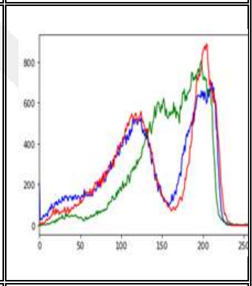
	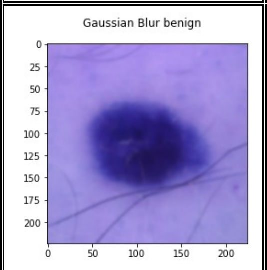	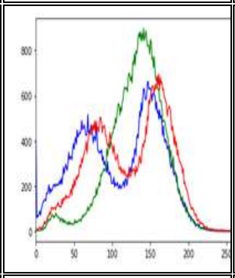	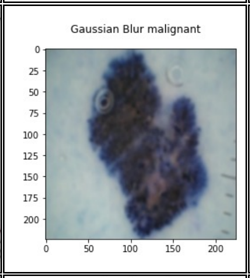	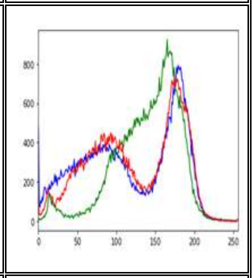
	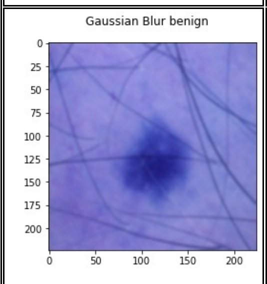	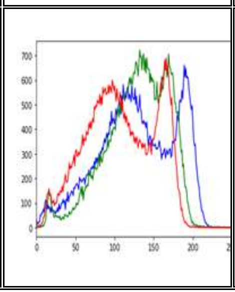	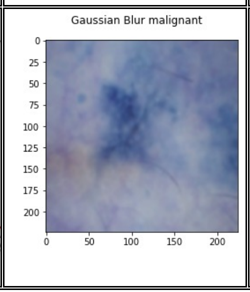	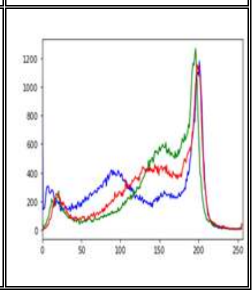

4.3.2.2 RGB to YCbCr color space results

The second step in the preprocessing stage is to transform colour Skin image samples from RGB to YCbCr for two classes in order to detect illness spots in skin cancer photos, as illustrated in the diagram below (Figure 4.2)

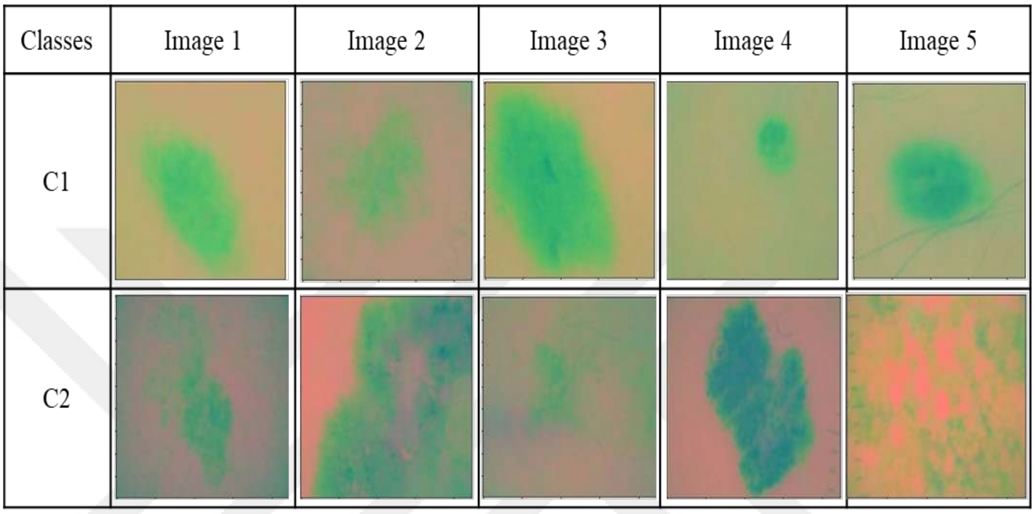

Figure 4.2 The results of YCbCr Color space

4.3.2.3 Fastest fourier transform (FTT) and morphology dilation operation (MDO)

The third step in fastest discrete Fourier transform (FFT) is preprocessing stage, and it is used to focus the edge characteristics of the pictures, potentially boosting the proposed system performance as discussed in the method 3.3. Figures 4.3 and Figure 4.4 showed the FFT method effect on all skin cancer sample photos for two classes

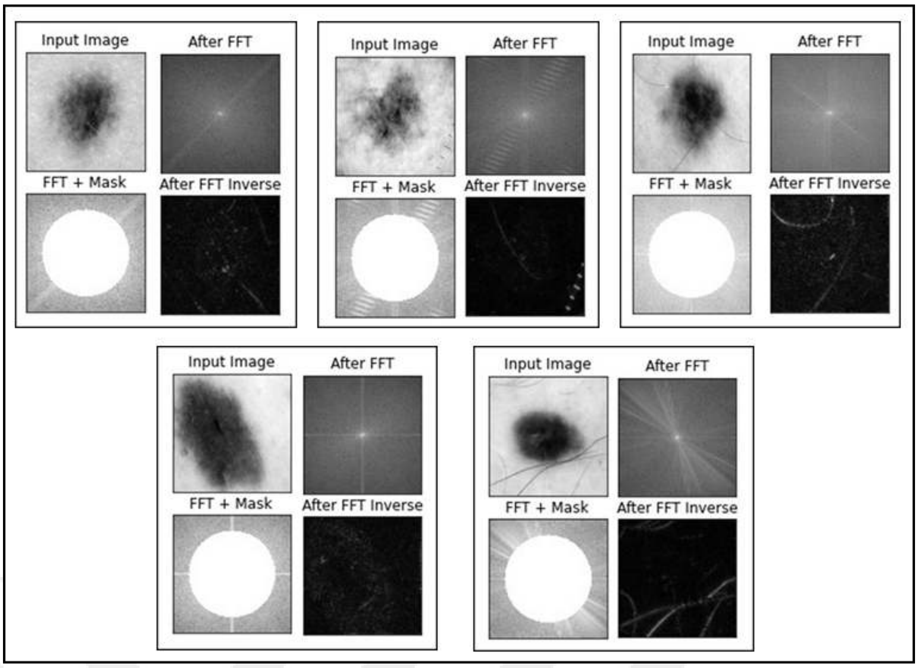

Figure 4.3 The results of class 1 images in fastest fourier transform stage

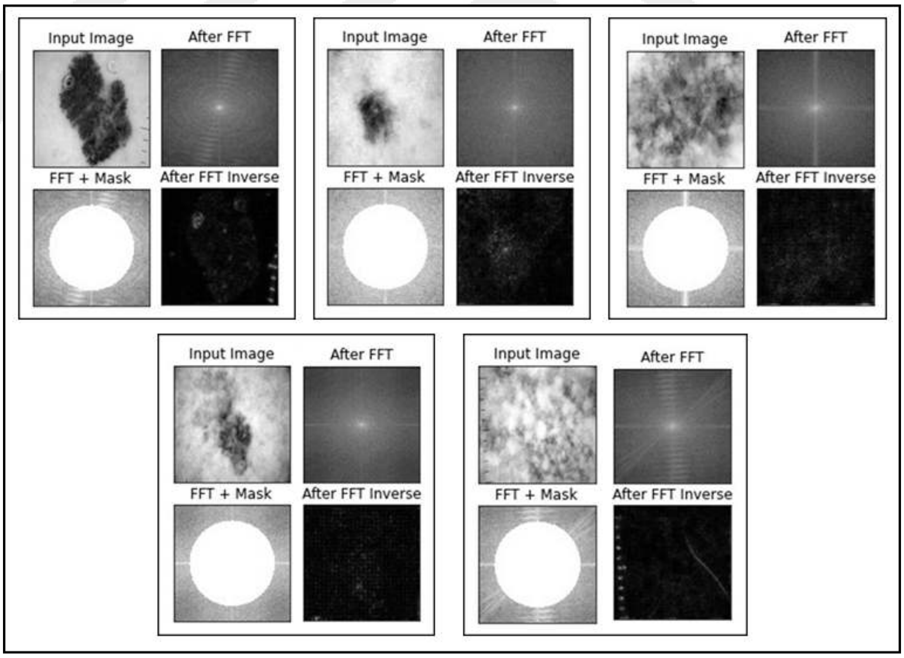

Figure 4.4 The results of class 1 images in fastest fourier transform stage.

The final step in the preparation stage is the morphological dilation operation, as indicated in method 3.4, which converts samples for all two classes of skin cancer pictures from YCbCr to grayscale images and makes ROI more obvious, as shown in Figure 4.3.

4.3.3 The classification stage

The proposed system is separated into two subsystems at current stage: a) machine learning-based detection and diagnosis of skin cancer illness utilising Nave Bayesian and Random Forest, with results shown in part (4.3.4.1). b) Represents deep learning-based detection and diagnosis of skin cancer illness using Deep CNN, with the outcomes of the Deep CNN system detailed in subsection (4.3.4.2)

4.3.3.1 Machine learning results

The initial subsystem is the classifying stage, which is centred on machine learning techniques and uses two of the most famous algorithms, Nave Bayesian (NB) and Random Forest (RF). The system is composed of two steps (feature extraction using the PCA algorithm and classification using the NB and RF algorithms), with the results of each step illustrated in subsection (i, ii, and iii).

i. The results of PCA

The PCA algorithm is employed to extract the features at the first stage of classification as discussed above. However, the valus the mean vectors for two classes of skin cancer images is culcalted by equation 3.4 and shown in Figure 4.5, Figure 4.6, Figure 4.7 and Figure 4.8

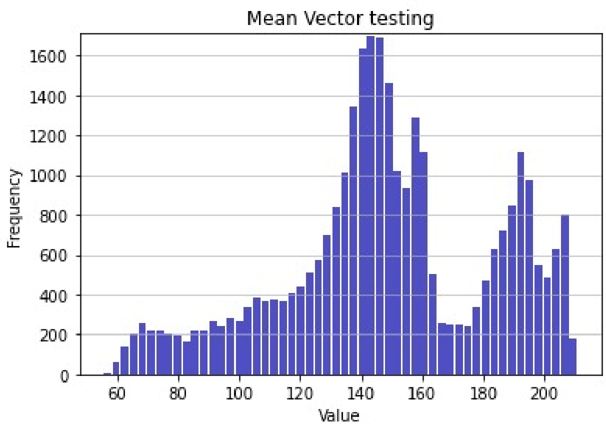

Figure 4.5 The mean vectors of skin cancer images for two classes

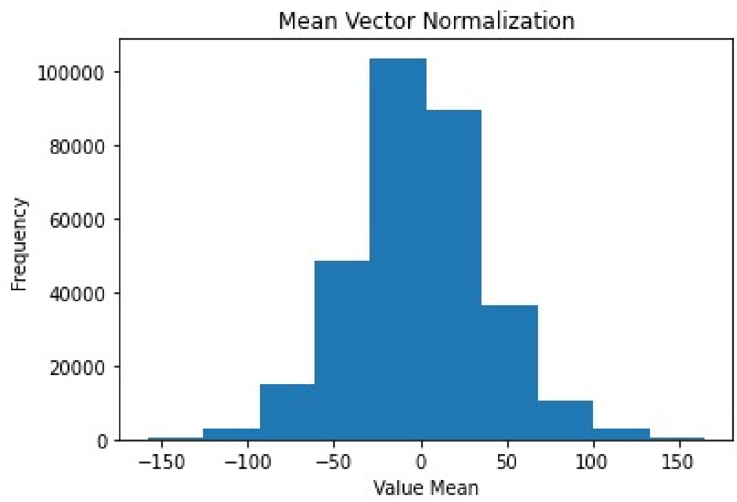

Figure 4.6 Mean normalization histogram for PCA algorithm

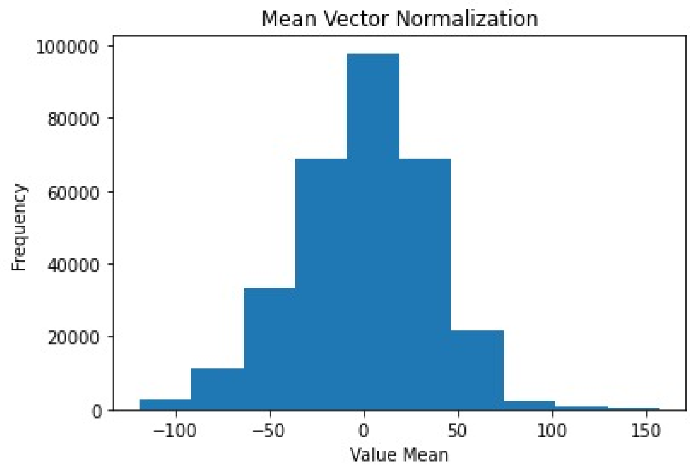

Figure 4.7 Mean normalization T histogram for PCA algorithm

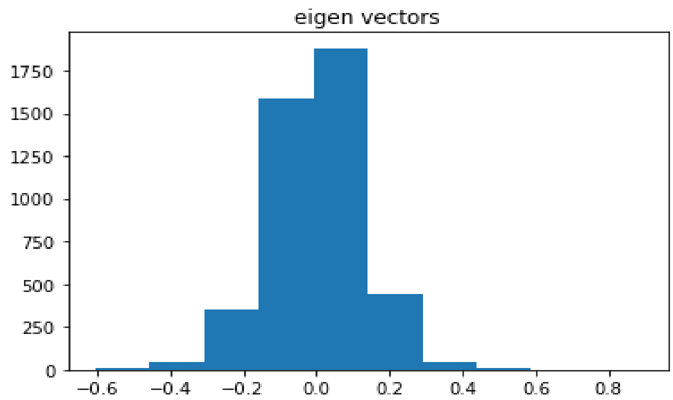

Figure 4.8 Features Eigen vector

ii. Naive Bayesian Results

It is one of the most effective machine algorithms which has been employed for image processing. It is result based on the values of the confusion matrix according to the discussion which has been done in the asbove chapters. Furthermore, bellow figure demonstrat the confusion matrix for the two classes of Skin cancer disease (Figure 4.9)

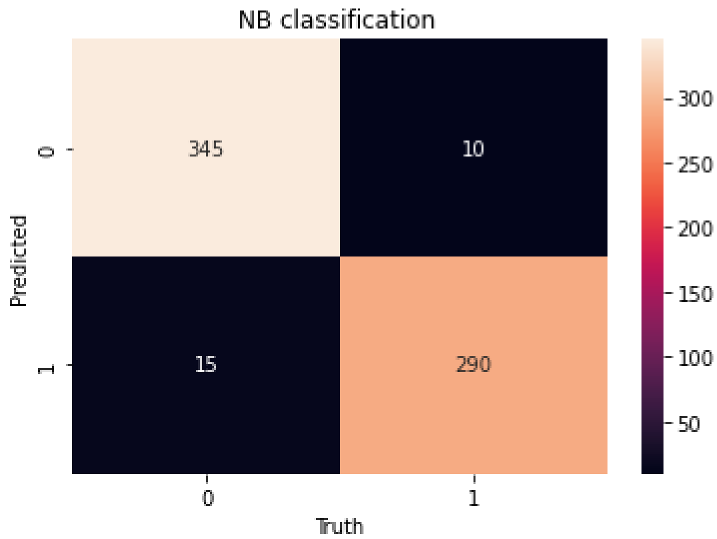

Figure 4.9 Naive Bayesian confusion matrix

Furthermore, according to the implementation it is observed that the results of the Naive Bayesian for class 1 were 0. 97% for both of F-score and recall, and precision of 0.96%.

Whereas, the results of the Naive Bayesian for class 2 were 0. 96% F-score and 0.95% recall, and precision of 0.97% However, the overall accuracy of Naive Bayesian is 0.96% for 660 testing images (Figure 4.10).

Whereas, the random forest also depended on the values of the confusion matrix as displayed in the bellow figure for two classes of Skin cancer disease

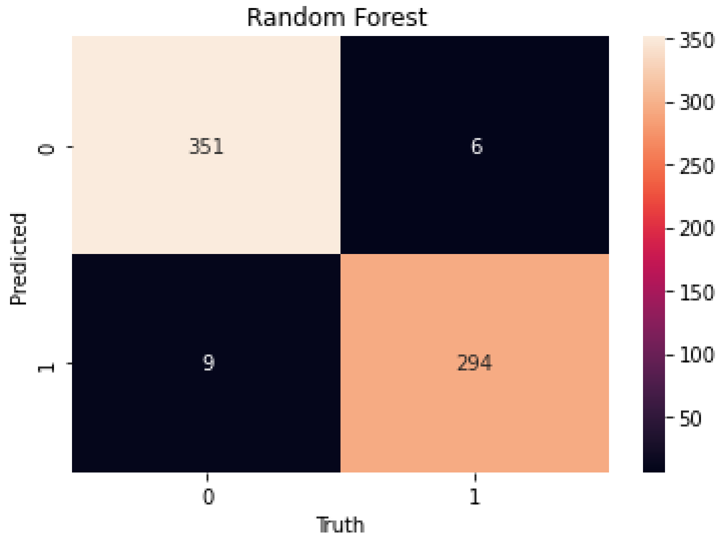

Figure 4.10 The confusion matrix for 2 classes by using Random Forest

Furthermore, according to the implementation it is observed that the results of the Random Forest for class 1 were 0.98% for both of F-score and recall, and precision of 0.97%. Whereas, the results of the Random Forest for class 2 were 0. 98% F-score and 0.98% recall, and precision of 0.98% However, the overall accuracy of Random Forest is 0.97% for 660 testing images.

Subsequently, the performance of both Naive Bayesian and Random Forest was a good in Skin cancer detection with accuracy of 96 % for Naive Bayesian and 97% for Random Forest. However, both of them are need to be improved to increase the accuracy of detection. Subsequently, by using 660 images for two classes, this comparison shows that the performance of Random Forest is better than the performance of Naive Bayesian in Skin cancer disease detection and diagnosis.

4.3.3.2 Deep learning results

The suggested DCNN system is the second subsystem, and it is categorized to use a deep learning method that employs the convolutional Neural network CNN algorithm. Furthermore, as the discussion which have been done above the dataset is spleted into training, testing and validation, wherein, the number of epoch=200 and the CNN algorithm running 200 for each epoch as shown in Table 4.3.

Table 4.3 Deep CNN results

# epoch	time	loss	accuracy
1	133s 3s	0.5105	0.4965
2	142s 3s	1.1439	0.4781
3	155s 3s	2.1378	0.4419
4	151s 3s	1.5248	0.4631
5	148s 3s	1.2351	0.4471
6	147s 3s	1.0412	0.4563
7	137s 3s	0.9163	0.4578
8	128s 3s	0.8270	0.4610
9	217s 4s	0.7784	0.4464
10	169s	0.7356	0.4419
11	139s 3s	0.6909	0.4502
12	114s 2s	0.6544	0.4581
13	71s 1s	0.6353	0.4550
14	78s 2s	0.6257	0.4471
15	78s 2s	0.6155	0.4432
16	82s 2s	0.5991	0.4483
17	85s 2s	0.5941	0.4444
18	80s 2s	0.5844	0.4469
19	81s 2s	0.5729	0.4525
20	86s 2s	0.5650	0.4556
21	85s 2s	0.5520	0.4648
---	---	---	---
200	950s 4s	6.30E-10	0.9931

The process of the Deep CNN layers is displayed in Table 4.4. The first convolution layer's output is max pooled, normalized, and sent as input to the 2nd layer of convolution. The 2nd layer's output is first normalized, then max pooled. The first convolution layer processes the input image with a 3×3 filter size and no padding. The pooling diagram is applied after the first convolution layer bypassing the input through the second convolution layer with a filter size of 3×3 and at stride 2. This procedure reduces the breadth and length of the data by a factor of four. The first pool layer's output is sent through the 2nd convolution layer and the max-pooling layer a second time. They employ start modules that carry many convolutionary kernels of varying sizes dimensions and collect the results throughout the depth dimension to extract features on multiple scales.

Table 4.4 The process of the Deep CNN layers

	Convolutional Layers (Benign)
	
Conv 2d	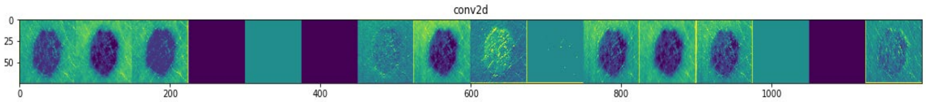
Max Pooling 2d	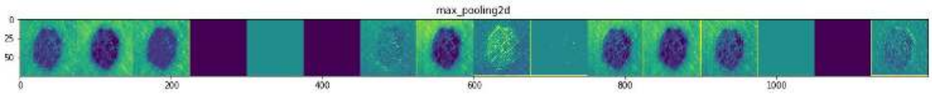
dropout	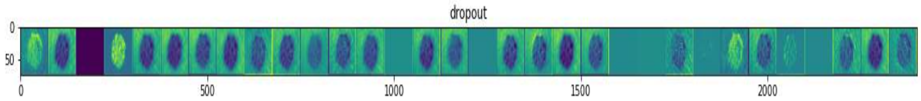
Conv 2d	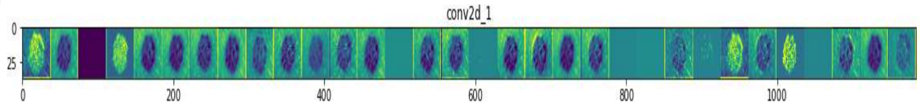
Max Pooling 2d	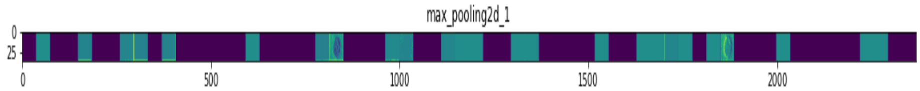
Conv 2d	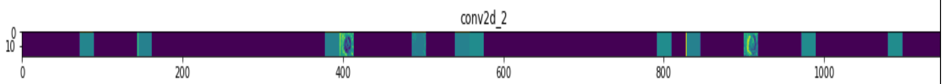
Max Pooling 2d	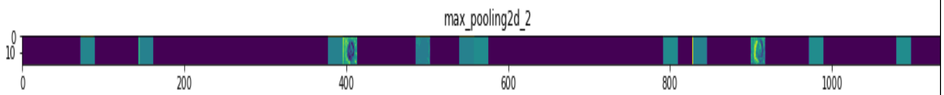
	Convolutional Layers (Malignant)
	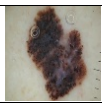
Conv2 d	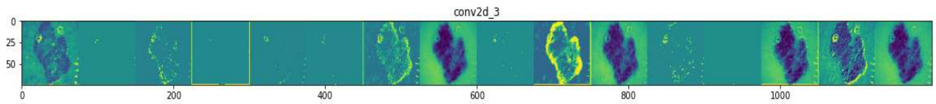
Max Pooling 2d	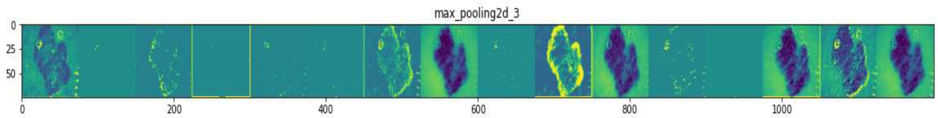

dropout	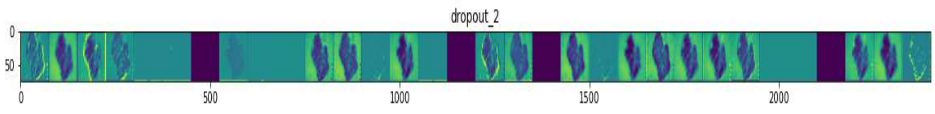
Conv2d	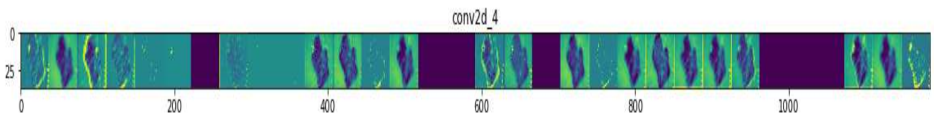
Max Pooling 2d	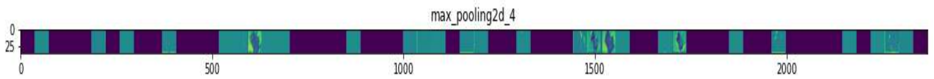
Conv2d	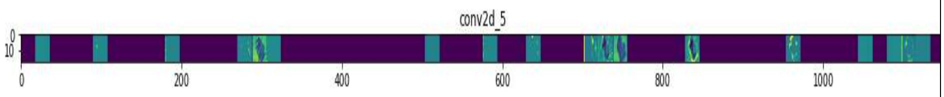
Max Pooling 2d	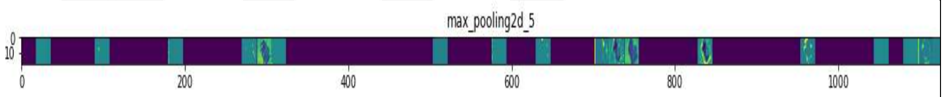

The histogram for both of training and validation are desipyed in the bellow Figure 4.11 and Figure 4.12

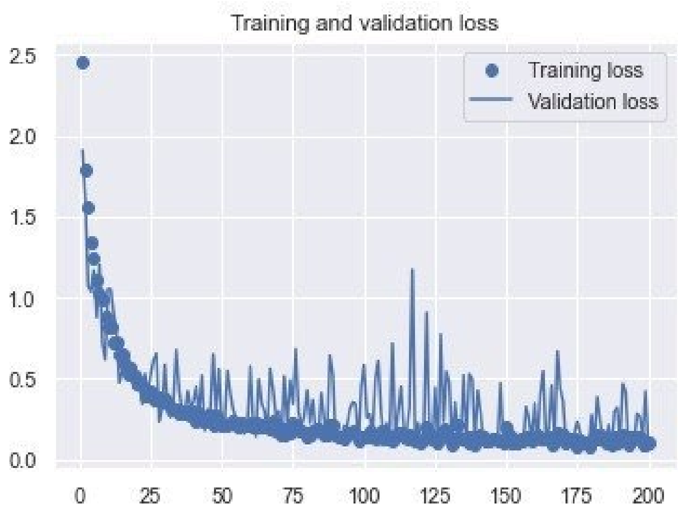

Figure 4.11 The loss in training and validation stage

Figure 4.12 Deep CNN accuracy

Finally, according to the obtained results, and during the comparision with machine learning it is observied that the Deep CNN is achieved the best results with accuracy of 99.51 with number of epoch of 200/200. (APPENDIX 1)

4.4 Analysis and Discussion

Since it is exposed to the outside environment and is very susceptible to illnesses, skin cancer detection has always been a hot topic. In most cases, proper and timely illness detection is critical to managing skin cancer since effective protective measures are frequently adopted following a right diagnosis.

To identify and diagnose skin cancer disorders, a variety of procedures have been proposed, developed, and deployed. The majority of them are unable to accurately identify and diagnose planet sickness. This study suggested, implemented, assessed, and compared an autonomous method for detecting and diagnosing early skin cancer disorders. Deep Conventional Neural Networks are used to power the system. The results, however, revealed that the suggested approach is effective in detecting and diagnosing early skin cancer disorders. The majority of approaches in the literature claim to have classification accuracy of 50% to 90%. When additional cases of skin cancer are added, such approaches may not perform as well as they do now.

Furthermore, as discussed in the preceding chapters, the system proposed comprises two components: first one is a DCNN-based system with twelve layers to improve detection and diagnostic precision. Second part is characterized by the implementation, design, testing, and evaluation of the most frequent and effective machine learning algorithms used for the detection and diagnosis of skin cancer disorders. Naive Bayes and Random Forest are the algorithms in question. In addition, the ISIS dataset was utilised to test and assess the performance of both subsystems, with 70% of the data being used for training and 30% for testing.

Following that, based on the acquired findings, it can be shown that the DCNN outperformed second part of machine learning and the widely used related research of (Daghrir *et al*. 2020, Kumar *et al.* 2018, Boman and Volminger 2018). DCNN and Machine Learning and Related Work comparasion are shown in Table 4. 5

Table 4.5 Proposed model comparasion with related work

Model	Techniques	Dataset	Accuracy%
Daghrir *et al.* 2020	CNN	ISIC	88.4%
Kumar1 *et al.* 2018	ANN	HAM10000	97.4
Boman and Volminger 2018	CNN	ISIC	91%
Machine learning	NB	ISIS	96
	RF	ISIS	97
Our proposed system	**DCNN**	**ISIS**	**99.5**

5 CONCLUSIONS AND FUTURE WORKS

5.1 Overview

Nowadays, detecting and diagnosing skin cancer in its early stages is a challenging challenge that women may face. Moreover, technology plays a significant role in the identification and diagnosis of skin cancer. As a result, an automated method for detecting and diagnosing early skin cancer illness is proposed. The system is made up of two primary subsystems, the first of which is on machine learning basis and second of which is on deep learning basis, which is this work's contribution

5.2 Conclusions

The suggested system is summarised in this chapter, and the following conclusions were drawn from the test results. The following are a few of the findings attained:

1- The proposed system is a strong methodology to detect and classify the skin cancer at early stage with the best accuracy.

2- The proposed system obtain the results by employing the Deep learning and Machine learning, each one used a different algorithm for classification and then compare the results of them with each other. The first sub-system is built based on the most efficient and effective machine learning classification methods which are Random Forest, and naïve Bayesian. Whereas, the second system is designed based on the Deep Convolutional Neural Network which achieved the highest results.

3- Both machine learning and deep learning algorithms were tested and evaluated on the same dataset of skin cancer illness images, with the same training size of 70% and 30% for testing.

4- Based on the acquired results, the NB is shown to be superior to the RF in machine learning. The NB attained a precision of 96 percent, while the RF acquired a precision of 97 percent.

5- The outcomes of both machine learning and deep learning were compared. Furthermore, the NB produced excellent results, with a 96 percent accuracy rate. In addition, the RF produced good results, with a 97 percent accuracy rate. In contrast to machine learning and the most comparable work, DCNN has produced the best results, with an accuracy of 99.5 percent, as shown in Table 4.5

5.3 Suggestions for Future Works

It is suggested that the following points be considered for future work:

- Using the suggested approach on a mobile device would allow for greater flexibility in the detection and diagnosis of skin cancer disorders.

- Experiment with the suggested approach on cancers that aren't addressed in this study.

REFERENCES

Al-Azawee, W. S., Abdel-Qader, I., & Abdel-Qader, J. 2015. Using morphological operations—Erosion based algorithm for edge detection. In 2015 IEEE International Conference on Electro/Information Technology (EIT) (pp. 521-525). IEEE.

Arora, J. & Agrawal, U. 2020. Classification of Maize leaf diseases from healthy leaves using Deep Forest. Journal of Artificial Intelligence and Systems, 2(1): 14-26.

Bayati, M. & Jabbar, S. 2015. Developing a spam email detector. Int J Eng Innov Technol, 5(2): 16-21.

Belgiu, M. & Drăguţ, L. 2016. Random forest in remote sensing: A review of applications and future directions. ISPRS journal of photogrammetry and remote sensing, 114: 24-31.

Boman, J. & Volminger, A. 2018. Evaluating a deep convolutional neural network for classification of skin cancer, Digitala Vetenskapliga Arkivet, 2018.

Chandel, R. & Gupta, G. 2013. Image filtering algorithms and techniques: A review. International Journal of Advanced Research in Computer Science and Software Engineering, 3(10).

Chow, L. S. & Paramesran, R. 2016. Review of medical image quality assessment. Biomedical signal processing and control, 27: 145-154.

Daghrir, J., Tlig, L., Bouchouicha, M., & Sayadi, M. 2020. Melanoma skin cancer detection using deep learning and classical machine learning techniques: A hybrid approach. In 2020 5th international conference on advanced technologies for signal and image processing (ATSIP) (pp. 1-5). IEEE.

Dunham, M. H. 2003. Data Mining – Introductory and Advanced Topics. Prentice Hall, Pearson Education, Upper Saddle River, New Jersey, MA 07458

Gedraite, E. S. & Hadad, M. 2011. Investigation on the effect of a Gaussian Blur in image filtering and segmentation. In Proceedings ELMAR-2011 (pp. 393-396). IEEE.

Gikunda, P. K. & Jouandeau, N. 2019. State-of-the-art convolutional neural networks for smart farms: A review. In Intelligent Computing-Proceedings of the Computing Conference (pp. 763-775). Springer, Cham.

Gobalakrishnan, N., Pradeep, K., Raman, C. J., Ali, L. J., & Gopinath, M. P. 2020. A systematic review on image processing and machine learning techniques for detecting plant diseases. In 2020 International Conference on Communication and Signal Processing (ICCSP) (pp. 0465-0468). IEEE..

Han, J., Pei, J. & Kamber, M. 2011. Data mining: concepts and techniques. Elsevier.

Hu, Z., Tang, J., Wang, Z., Zhang, K., Zhang, L., & Sun, Q. 2018. Deep learning for image-based cancer detection and diagnosis− A survey. Pattern Recognition, 83: 134-149.

Hudson, D. L. & Cohen, M. E. 2003. The role of information technology in disease management. In 4th International IEEE EMBS Special Topic Conference on Information Technology Applications in Biomedicine, 2003. (pp. 62-65). IEEE.

Ibrahim, A. O., Shamsuddin, S. M., & Qasem, S. N. 2015. Hybrid NSGA-II optimization for improving the three-term BP network for multiclass classification problems. Journal of Information and Communication Technology, 14: 21-38.

Jain, S. & Pise, N. 2015. Computer aided melanoma skin cancer detection using image processing. Procedia Computer Science, 48: 735-740.

Kaur, S. & Jindal, S. 2016. A survey on machine learning algorithms. Int J Innovative Res Adv Eng (IJIRAE), 3(11): 2349-2763.

Kaushik, C. S. H., Gautam, T., & Elamaran, V. 2014. A tutorial review on discrete fourier transform with data compression application. In 2014 International Conference on Green Computing Communication and Electrical Engineering (ICGCCEE) (pp. 1-6). IEEE.

Kim, S. B., Han, K. S., Rim, H. C., & Myaeng, S. H. 2006. Some effective techniques for naive bayes text classification. IEEE transactions on knowledge and data engineering, 18(11): 1457-1466.

Kingma, D. P. & Ba, J. 2014. Adam: A method for stochastic optimization. arXiv preprint arXiv:1412.6980.

Kolkur, S., Kalbande, D., Shimpi, P., Bapat, C., & Jatakia, J. 2017. Human skin detection using RGB, HSV and YCbCr color models. arXiv preprint arXiv:1708.02694.

Kulkarni, V. Y., Petare, M., & Sinha, P. K. 2014. Analyzing random forest classifier with different split measures. In Proceedings of the Second International Conference on

Soft Computing for Problem Solving (SocProS 2012), December 28-30, 2012 (pp. 691-699). Springer, New Delhi..

Kumar, M. N., Koushik, K. V. S., & Deepak, K. 2018. Prediction of heart diseases using data mining and machine learning algorithms and tools. International Journal of Scientific Research in Computer Science, Engineering and Information Technology, 3(3): 887-898.

Kumar, M., Alshehri, M., AlGhamdi, R., Sharma, P., & Deep, V. 2020. A de-ann inspired skin cancer detection approach using fuzzy c-means clustering. Mobile Networks and Applications, 25: 1319-1329.

Lee, C. Y., Gallagher, P. W., & Tu, Z. 2016. Generalizing pooling functions in convolutional neural networks: Mixed, gated, and tree. In Artificial intelligence and statistics (pp. 464-472). PMLR.

Mansutti, G., Mobashsher, A. T., & Abbosh, A. M. 2018. Millimeter-wave substrate integrated waveguide probe for near-field skin cancer detection. In 2018 Australian Microwave Symposium (AMS) (pp. 81-82). IEEE.

Mecheter, I., Alic, L., Abbod, M., Amira, A., & Ji, J. 2020. MR image-based attenuation correction of brain PET imaging: review of literature on machine learning approaches for segmentation. Journal of Digital Imaging, 33(5): 1224-1241.

Mitra, S. & Acharya, T. 2005. Data mining: multimedia, soft computing, and bioinformatics. John Wiley & Sons.

Monika, M. K., Vignesh, N. A., Kumari, C. U., Kumar, M. N. V. S. S., & Lydia, E. L. 2020. Skin cancer detection and classification using machine learning. Materials Today: Proceedings, 33: 4266-4270.

Munir, K., Elahi, H., Ayub, A., Frezza, F., & Rizzi, A. 2019. Cancer diagnosis using deep learning: a bibliographic review. Cancers, 11(9), 1235.

Nahata, H. & Singh, S. P. 2020. Deep learning solutions for skin cancer detection and diagnosis. In Machine Learning with Health Care Perspective (pp. 159-182). Springer, Cham.

Naji, G. W. & Al-Tuwaijari, J. M. 2018. Satellite Images Multiple Data Using Clustering Techniques. Iraqi Journal of Information Technology. V: 9(2).

Olbrys, J. & Mursztyn, M. 2019. Measuring stock market resiliency with Discrete Fourier Transform for high frequency data. Physica A: Statistical Mechanics and Its Applications, 513: 248-256.

Patil, P. M. and Patil, Y. M. 2012. "Robust Skin Colour Detection and Tracking Algorithm", International Journal of Engineering Research and Technology Vol. 1. No.8 (October-2012), ISSN: 2278-0181 (2012).

Poorani, M., Prathiba, T. and Ravindran, G. 2013 "Integrated Feature Extraction for Image Retrieval", International Journal of Computer Science and Mobile Computing, pp. 28-35,

Rasheed, M. H., Salih, O. M., Siddeq, M. M., & Rodrigues, M. A. 2020. Image compression based on 2D Discrete Fourier Transform and matrix minimization algorithm. Array, 6, 100024.

Reddy, A., Indragandhi, V., Ravi, L., & Subramaniyaswamy, V. 2019. Detection of Cracks and damage in wind turbine blades using artificial intelligence-based image analytics. Measurement, 147: 106823.

Rey-Barroso, L., Peña-Gutiérrez, S., Yáñez, C., Burgos-Fernández, F. J., Vilaseca, M., & Royo, S. 2021. Optical Technologies for the Improvement of Skin Cancer Diagnosis: A Review. Sensors, 21(1): 252.

Rock, C. L., Thomson, C., Gansler, T., Gapstur, S. M., McCullough, M. L., Patel, A. V., & Doyle, C. 2020. American Cancer Society guideline for diet and physical activity for cancer prevention. CA: a cancer journal for clinicians, 70(4): 245-271.

Saba, T. 2020. Recent advancement in cancer detection using machine learning: Systematic survey of decades, comparisons and challenges. Journal of Infection and Public Health, 13(9): 1274-1289.

Santra, A. K. & Christy, C. J. 2012. Genetic algorithm and confusion matrix for document clustering. International Journal of Computer Science Issues (IJCSI), 9(1): 322.

Shrestha, A. & Mahmood, A. 2019. Review of deep learning algorithms and architectures. IEEE access, 7: 53040-53065.

Singh, A., Singh, M., & Singh, B. 2016. Face detection and eyes extraction using sobel edge detection and morphological operations. In 2016 Conference on Advances in Signal Processing (CASP) (pp. 295-300). IEEE.

Soni, A. & Singh, A. P. 2020. Automatic Pulmonary Cancer Detection using Prewitt & Morphological Dilation. In 2nd International Conference on Data, Engineering and Applications (IDEA) (pp. 1-6). IEEE.

Sultana, N. N. & Puhan, N. B. 2018. Recent deep learning methods for melanoma detection: a review. In International Conference on Mathematics and Computing (pp. 118-132). Springer, Singapore.

Tiwari, S., Shukla, V. P., Singh, A. K., & Biradar, S. R. 2013. Review of motion blur estimation techniques. Journal of Image and Graphics, 1(4): 176-184.

Wang, A., Zhang, W., & Wei, X. 2019. A review on weed detection using ground-based machine vision and image processing techniques. Computers and electronics in agriculture, 158: 226-240.

Xia, C., Yang, S., Huang, M., Zhu, Q., Guo, Y., & Qin, J. 2019. Maize seed classification using hyperspectral image coupled with multi-linear discriminant analysis. Infrared Physics & Technology, 103: 103077.

Yin, H. & Chaoyang, Z. 2011. An improved bayesian algorithm for filtering spam e-mail. In 2011 2nd International Symposium on Intelligence Information Processing and Trusted Computing (pp. 87-90). IEEE.

Younis, H., Bhatti, M. H., & Azeem, M. 2019. Classification of skin cancer dermoscopy images using transfer learning. In 2019 15th International Conference on Emerging Technologies (ICET) (pp. 1-4). IEEE.

Zahradnikova, B., Duchovicova, S., & Schreiber, P. 2015. Image mining: review and new challenges. International Journal of Advanced Computer Science and Applications, 6(7): 242-246.

Zhang, S., Zhang, S., Zhang, C., Wang, X., & Shi, Y. 2019. Cucumber leaf disease identification with global pooling dilated convolutional neural network. Computers and Electronics in Agriculture, 162: 422-430

APPENDICES

APPENDIX 1. The accuracy pattern of 200 rounds epoch

APPENDIX 1. The accuracy pattern of 200 rounds epoch

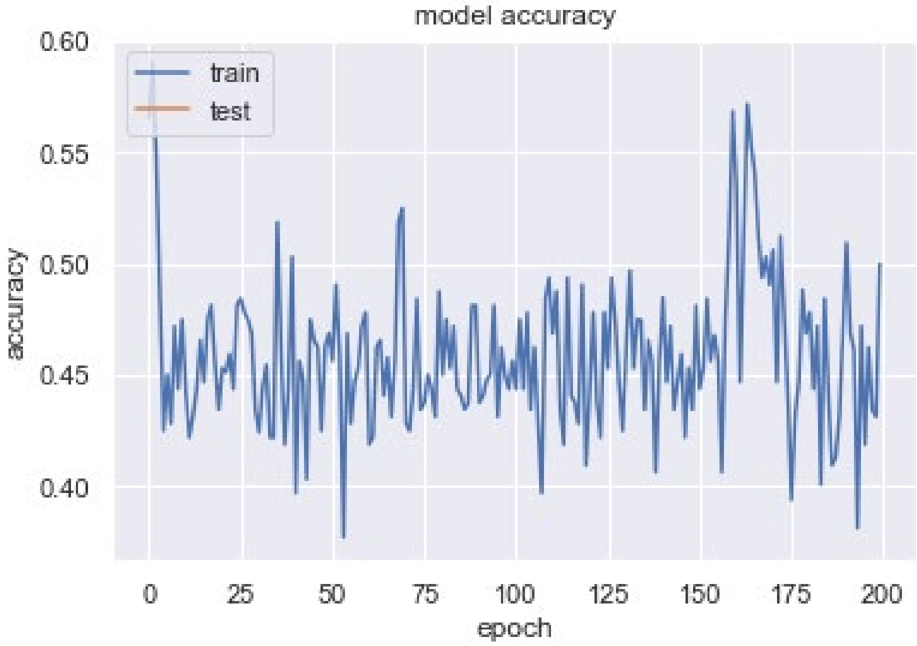

CURRICULUM VITAE

Personal Information

Name and Surname	: Mohammed Hani Shakir KFASHI

Education

MSc	Çankırı Karatekin University Faculty of Engineering Electrical and Electronics Engineering	2020-Present
Undergraduate	Al-Ma'Mon University Faculty of Engineering Computer Techniques Engineering	2011-2015